

Thesis for the degree of Doctor of Philosophy

Beam-Based Error Identification and Correction Methods  
for Particle Accelerators

TOBIAS PERSSON

Department of Fundamental Physics  
CHALMERS UNIVERSITY OF TECHNOLOGY  
Göteborg, Sweden 2014

Beam-Based Error Identification and Correction Methods for  
Particle Accelerators  
TOBIAS PERSSON  
ISBN 978-91-7597-026-4

© TOBIAS PERSSON, 2014.

Doktorsavhandling vid Chalmers tekniska högskola  
Ny serie nr 3707  
ISSN 0346-718X

Department of Fundamental Physics  
Chalmers University of Technology  
SE-412 96 Göteborg, Sweden  
Telephone: +46 (0)31-772 1000

Typeset in L<sup>A</sup>T<sub>E</sub>X; figures created using MATLAB, Gnuplot.

Chalmers reproservice  
Göteborg, Sweden 2014

Beam-Based Error Identification and Correction Methods for  
Particle Accelerators  
TOBIAS PERSSON  
Department of Fundamental Physics  
Chalmers University of Technology

## ABSTRACT

Modern particle accelerators have tight tolerances on the acceptable deviation from their desired machine parameters. The control of the parameters is of crucial importance for safe machine operation and performance. This thesis focuses on beam-based methods and algorithms to identify and correct errors in particle accelerators. The optics measurements and corrections of the Large Hadron Collider (LHC), which resulted in an unprecedented low  $\beta$ -beat for a hadron collider is described. The transverse coupling is another parameter which is of importance to control. Improvement in the reconstruction of the coupling from turn-by-turn data has resulted in a significant decrease of the measurement uncertainty. An automatic coupling correction method, which is based on the injected beam oscillations, has been successfully used in normal operation of the LHC. Furthermore, a new method to measure and correct chromatic coupling that was applied to the LHC, is described. It resulted in a decrease of the chromatic coupling by a factor  $\sim 2$  for both beams. The good control of the optics is a significant part of the success of the LHC and hence contributed to the discovery of the Higgs particle.

Following the discovery of the Higgs particle there is a demand for precise measurements of its properties in a lepton collider. Compact Linear Collider (CLIC), an electron-positron collider aiming at collision energies up to 3 TeV, is one of the leading candidates. The acceleration in CLIC relies on a two-beam acceleration scheme where one of the beams, referred to as the Drive Beam, is decelerated while transferring its energy to the Main Beam. This scheme puts tight constraints on the parameters of the Drive Beam in terms of beam current, phase and bunch length. In CLIC Test Facility 3 (CTF3) the mechanisms behind the observed drifts of these parameters have been studied in detail. The findings have shown that these drifts are mainly linked to variations in the amplitude of the Radio Frequency (RF). A feedback to mitigate the RF-amplitude fluctuations has been implemented and is described in detail. In conjunction with a dedicated energy feedback it reduces the energy variation by a factor  $\sim 3$ . Together with precise machine tuning this has resulted in a beam current stability very close to the CLIC requirement. The beam phase stability is improved through a feedback operating on the two first klystrons in the CTF3 injector. Two-beam acceleration at the nominal CLIC gradient of 100 MV/m and above has been demonstrated in CTF3. These results, and other recent achievements in CTF3, are presented in this thesis.

**Keywords:** Accelerators, Accelerator Optics, CLIC, CTF3, Emittance, Feedback, LHC, Pulse Compressor, Radio Frequency, Two-beam acceleration



# List of Papers

This thesis is based on the papers listed below. They are referred to in the text by their Roman numerals. List of articles included in this thesis:

## I Record low $\beta$ -beating in the LHC

R. Tomas, T. Bach, R. Calaga, A. Langner, Y. I. Levinsen, E. H. Maclean, T. H. B. Persson, P. K. Skowronski, M. Strzelczyk, G. Vanbavinckhove [CERN, Geneva, Switzerland]  
*Phys. Rev. ST Accel. Beams* 15, 091001, 2012

## II Commissioning and Operation at $\beta^* = 1000$ m in the LHC

H. Burkhardt, T. Persson, R. Tomas, J. Wenninger [CERN, Geneva, Switzerland] S. Cavalier [LAL, Orsay, France]  
*Proceedings of IPAC'13, Shanghai, China, pp. 1982-1984, 2013*

## III Improved Control of the Betatron Coupling in the Large Hadron Collider

T. Persson, R. Tomas [CERN, Geneva, Switzerland]  
*Accepted for publication in Phys. Rev. ST Accel. Beams*

## IV Automatic Correction of Betatron Coupling in the LHC using Injection Oscillations

T. Persson, T. Bach, D. Jacquet, V. Kain, Y. I. Levinsen, E. H. Maclean, M. J. McAteer, P. K. Skowronski, R. Tomas, G. Vanbavinckhove [CERN, Geneva, Switzerland] R. Miyamoto [ESS, Lund, Sweden]  
*Proceedings of IPAC'13, Shanghai, China, pp. 1979-1981, 2013*

## V Chromatic Coupling Correction in the Large Hadron Collider <sup>1</sup>

T. Persson, Y. Inntjore Levinsen, R. Tomas Garcia, E. H. Maclean [CERN, Geneva, Switzerland]  
*Phys. Rev. ST Accel. Beams* 16 081003, 2013

## VI Drive beam stability studies and stabilization algorithms in CTF3

T. Persson, R. Corsini, P. Skowronski  
*Nuclear Instruments and Methods in Physics Research Section A: Accelerators, Spectrometers, Detectors and Associated Equipment, Volume 735, Pages 152-156, 21 January 2014*

## VII Beam Stability at CTF3

T. Persson, R. Corsini, P. Skowronski [CERN, Geneva, Switzerland]  
*Proceedings of IPAC'12, New Orleans, USA, pp. 1890-1892, 2012.*

---

<sup>1</sup>Awarded with the Editors' Suggestion

### VIII **Experimental Verification of the CLIC Two-Beam Acceleration Technology in CTF3**

P. K. Skowronski , A. Andersson, J. Barranco, B. Constance, R. Corsini, A. Dubrovskiy, S. Dobert, W. Farabolini, E. Ikarios, F. Tecker [CERN, Geneva, Switzerland] M. Jacewicz, A. Palaia, R. J. M. Y. Ruber [Uppsala University, Uppsala, Sweden] R. L. Lillestol [University of Oslo, Oslo, Norway] T. Persson [Chalmers University of Technology, Gothenburg, Sweden] *Proceedings of IPAC'13, Shanghai, China, pp. 1436-1438, 2013*

### IX **Two Beam Test Stand Experiments in the CTF3 Facility**

W. Farabolini, F. Peauger [CEA/DSM/IRFU, France] J. Barranco, S. Bettoni, B. Constance, R. Corsini, M. Csatari, A. Dubrovskiy, S. Dobert C. Hessler , T. Persson, G. Riddone, P. K. Skowronski, F. Tecker [CERN, Geneva, Switzerland] D. Gudkov, A. Solodko [JINR, Dubna, Moscow Region, Russia] M. Jacewicz, T. Muranaka, A. Palaia, R. J. M. Y. Ruber, V. G. Ziemann [Uppsala University, Uppsala, Sweden] *Proceedings of IPAC'11, San Sebastián, Spain, pp. 29-31, 2011*

List of articles I have contributed to but which are not included in the thesis:

- X **The Drive Beam Phase Stability in CTF3 and its Relation to the Bunch Compression Factor**  
E. Ikarios, A. Andersson, J. Barranco, B. Constance, R. Corsini, A. Gerbershagen, T. Persson, P. K. Skowronski, F. Tecker [CERN, Geneva, Switzerland]  
*Proceedings of IPAC'13, Shanghai, China, pp. 1655-1657, 2013*
- XI **Review of the Drive Beam Stabilization in the CLIC Test Facility CTF3**  
A. Dubrovskiy, L. Malina, P. K. Skowronski, F. Tecker [CERN, Geneva, Switzerland] T. Persson [Chalmers University of Technology, Gothenburg, Sweden]  
*Proceedings of IPAC'13, Shanghai, China, pp. 2666-2668, 2013*
- XII **Measurement of LHC non-linear observables using kicked beams**  
E. H. Maclean, R. Tomas, F. Schmidt, and T. H. B. Persson [CERN, Geneva, Switzerland]  
*Under review for Phys. Rev. ST Accel. Beams*
- XIII **Determination of Octupole and Sextupole Polarities in the LHC**  
M. J. McAteer, Y. I. Levinsen, E. H. Maclean, T. Persson, P. K. Skowronski, R.J. Steinhagen, R. Tomas [CERN, Geneva, Switzerland]  
*Proceedings of IPAC'13, Shanghai, China, pp. 655-657, 2013*
- XIV **Optics Performance of the LHC During the 2012 Run**  
P. K. Skowronski, T. Bach, M. Giovannozzi, A. Langner, Y. I. Levinsen, E. H. Maclean, S. Redaelli, T. Risselada, M. Solfaroli Camillocci, R. Tomas, G. Vanbavinckhove [CERN, Geneva, Switzerland] M. J. McAteer [The University of Texas at Austin, Austin, USA] R. Miyamoto [ESS, Lund, Sweden] T. Persson [Chalmers University of Technology, Sweden]  
*Proceedings of IPAC'13, Shanghai, China, pp. 1435-1437, 2013*
- XV **Operating the LHC Off-momentum for p-Pb Collisions**  
R. Versteegen, R. Bruce, J. M. Jowett, A. Langner, Y. I. Levinsen, E. H. Maclean, M. J. McAteer, S. Redaelli, B. Salvachua, P. K. Skowronski, M. Solfaroli Camillocci, R. Tomas, G. Valentino, J. Wenninger [CERN, Geneva, Switzerland] T. Persson [Chalmers University of Technology, Sweden] S. M. White [BNL, Upton, Long Island, New York, USA]  
*Proceedings of IPAC'13, Shanghai, China, pp. 1439-1441, 2013*

---

**XVI Understanding the Tune, Coupling, and Chromaticity Dependence of the LHC on Landau Octupole Powering**

E. H. Maclean, M. Giovannozzi, W. Herr, Y. I. Levinsen, G. Papotti, T. Persson, P. K. Skowronski, R. Tomas, J. Wenninger [CERN, Geneva, Switzerland]

*Proceedings of IPAC'13, Shanghai, China, pp. 1976-1978, 2013*

# Contents

List of papers . . . . .	v
Table of content . . . . .	xi
<b>1 Introduction</b>	<b>1</b>
1.1 The Scope and Outline of the Thesis . . . . .	2
1.2 LHC - A Multi Purpose Machine . . . . .	3
1.3 Hadron and Lepton Colliders: A Love Story . . . . .	4
1.4 Which Future Machine? . . . . .	6
<b>2 Introduction to Beam Physics</b>	<b>9</b>
2.1 Introduction . . . . .	9
2.2 Beam and Optics Parameters . . . . .	11
2.2.1 Betatron Tune . . . . .	11
2.2.2 Resonances . . . . .	11
2.2.3 $\beta$ -function . . . . .	12
2.2.4 Dispersion . . . . .	13
2.2.5 Chromaticity . . . . .	13
2.2.6 Emittance . . . . .	13
2.3 Decoherence . . . . .	15
2.4 Non-linear Magnetic Multipoles . . . . .	16
2.5 Coupling . . . . .	18
2.5.1 Parametrization of Linear Coupling . . . . .	18
2.6 Resonance Driving Terms . . . . .	19
<b>3 Optics Corrections in the LHC</b>	<b>21</b>
3.1 Optics Measurements Methods . . . . .	21
3.1.1 Exciting the Beam . . . . .	21
3.1.2 Measuring the Phase . . . . .	22
3.1.3 Measuring the $\beta$ -function . . . . .	22
3.1.4 K-modulation . . . . .	22
3.1.5 Measuring Dispersion . . . . .	23
3.2 Correction Methods . . . . .	24
3.2.1 Local Corrections . . . . .	24
3.2.2 Global Corrections . . . . .	25
3.3 Correction Procedure . . . . .	25

3.4	Results . . . . .	26
3.4.1	Nominal Optics . . . . .	26
3.4.2	High $\beta^*$ . . . . .	26
3.4.2.1	$\beta^* = 90$ m . . . . .	26
3.4.2.2	$\beta^* = 500$ m . . . . .	27
3.4.2.3	$\beta^* = 1000$ m . . . . .	27
<b>4</b>	<b>Linear Coupling Corrections</b>	<b>31</b>
4.1	Coupled Motion . . . . .	31
4.2	From $k_s$ to $C^\pm$ . . . . .	33
4.3	Measuring the $f_{1001}$ and $f_{1010}$ . . . . .	34
4.4	Correction Procedure in the LHC . . . . .	38
4.4.1	Local Coupling Correction . . . . .	38
4.4.2	Global Corrections . . . . .	39
4.4.2.1	Automatic Coupling Corrections Based on In- jection Oscillations . . . . .	39
4.4.2.2	Coupling Feedback . . . . .	41
4.4.3	The Influence of Coupling on $\beta$ -beat . . . . .	41
<b>5</b>	<b>Chromatic coupling</b>	<b>43</b>
5.1	From Sextupolar Fields to Chromatic Coupling . . . . .	44
5.2	Motivation . . . . .	45
5.3	Measurement and Correction Procedure . . . . .	45
<b>6</b>	<b>CLIC</b>	<b>47</b>
6.1	Requirements that Drive the Design . . . . .	47
6.1.1	Reaching the TeV-scale . . . . .	47
6.1.2	Reaching High Luminosity . . . . .	48
6.2	Layout . . . . .	49
<b>7</b>	<b>Experimental Verification at CTF3</b>	<b>51</b>
7.1	Layout of CTF3 . . . . .	52
7.1.1	Drive Beam Generation . . . . .	53
7.1.1.1	Emittance Preservation in the Combiner Ring . . . . .	54
7.2	Beam Stability at CTF3 . . . . .	55
7.2.1	Motivation . . . . .	55
7.2.2	Relation to CLIC . . . . .	56
7.2.3	Beam Current Variation . . . . .	56
7.2.4	Phase and Bunch Length Variation . . . . .	56
7.3	Two-beam Acceleration . . . . .	57
<b>8</b>	<b>Conclusion and Outlook</b>	<b>59</b>
<b>9</b>	<b>Abbreviations and Acronyms</b>	<b>63</b>

Contents

---

<b>Bibliography</b>	<b>71</b>
<b>Acknowledgment</b>	<b>74</b>
<b>A Resonance Driving Terms</b>	<b>75</b>



# Chapter 1

## Introduction

In November 2013 it was announced that Peter Higgs and François Englert were awarded the Nobel Prize in physics. They were awarded for their contribution to the construction of the theory predicting the Higgs boson. In the announcement the Large Hadron Collider (LHC) was credited for producing the collisions that enabled the two experiments, A Toroidal LHC Apparatus (ATLAS) and Compact Muon Solenoid (CMS), to discover the Higgs particle [1]. The experimental discovery of the Higgs particle is the result of work by thousands of people, carried out over almost three decades. The first workshop held on the topic of a superconducting hadron accelerator in the Large Electron Positron (LEP) tunnel was held in 1984 [2]. This demonstrates the time scale of the modern particle physics experiments and the necessity to already now start developing the tools which need to be ready in 20 years.

In 2013, after three years of almost constant running, the LHC was shut down for an upgrade to be able to provide collisions of at least 13 TeV center of mass energy. At these higher energies there is hope to find signs of new physics beyond what is described by the standard model. Examples of new physics predicted by theories are supersymmetry and extra dimensions [3].

This thesis consists of two parts. The first part focuses on optics corrections in the LHC. The good control of the optics in the LHC is one of the reasons for its success. In being a part of the success of the LHC it contributed to the exploration of a new energy scale and the discovery of a new boson. The particles and physics found, or not found, are of great importance to decide for the next generation colliders.

The second part describes the feasibility demonstration of Compact Linear Collider (CLIC), a proposed next generation  $e^+e^-$  collider, carried out at CLIC Test Facility 3 (CTF3). In particular it will focus on the methods and feedbacks developed in order to experimentally demonstrate crucial beam parameters.

This chapter begins with a description of the scope and outline of the thesis, followed by an introduction to the LHC and a description of the complementarity between hadron and lepton machines. Finally, a comparison between

different options for the next generation lepton colliders is given.

## 1.1 The Scope and Outline of the Thesis

A major challenge in accelerator physics and engineering is to achieve and preserve good beam conditions. The beam is deviating from the design behaviour in case of for example errors in magnets, powering, vibration, or Radio Frequency (RF) fluctuations. Fortunately, the beam itself is an excellent probe to identify errors. Studying the beam's behaviour, using the available beam instrumentation and appropriate algorithms is crucial for identifying error sources. When the errors' influence on the beam is established, the error source might be corrected or an approach to mitigate the problem can be taken. The general quest of this thesis is to develop algorithms and methods, based on beam measurements, that find errors and drifts in accelerators and to implement methods to mitigate these errors. The applied algorithms are also, when appropriate, compared to simulations in order to validate them. The possibility to access the underlying variables and compare them to the reconstructed quantity is the big advantage of simulations.

In chapter 2 an introduction to the physics that govern the behaviour of the particles in an accelerator will be given. It will provide the fundamental concepts which will be needed to understand the measurements and corrections described in the rest of the thesis.

The magnetic fields of the LHC magnets are not known with enough precision to allow for normal operation without first performing a beam-based measurement and correction. From the beam-based measurements it is possible to localise some errors while others need to be mitigated through a global approach. This is done during the optics commissioning described in detail in chapter 3.

After the commissioning some parameters like the transverse coupling is observed to vary in time. In chapter 4 a method to measure and correct the global transverse coupling based on the injection oscillations is described. Improvements in the algorithms used to reconstruct the coupling are also presented. Furthermore, the design of a new feedback to control the linear coupling throughout the magnetic cycle will also be given.

Higher order field errors are an inherent consequence of the superconducting dipole magnets installed in the LHC. As a consequence, spool piece magnets are installed for local compensation of the magnetic fields [4]. Some of the higher order components, which are not fully corrected, give rise to an energy dependent coupling, termed chromatic coupling. A novel beam-based method to measure and correct the chromatic coupling is described in chapter 5.

Most of the stability and error identification challenges are common between circular and linear machines. However, there are some fundamental differences. These differences originate mainly from the fact that linear machines operate in a pulsed mode, meaning that a new beam arrives at the repetition rate of

the machine. Typical repetition rates range from 0.8 Hz to 100[Hz]. Each pulse might for example have a different current or energy. In a circular machine beam properties like the beam current remains constant as long as no losses occur. CLIC is an example of a future linear collider operated in a pulsed mode. An introduction to the CLIC concept and its challenges are given in chapter 6. In chapter 7 studies to identify observed beam drifts in CTF3 are presented together with implemented feedbacks to mitigate them. Other beam-based studies important for the demonstration of the CLIC concept are also presented.

Finally, in chapter 8 a conclusion of the presented work will be given. It will try to summarize the most important results and discuss their impact. An outlook on future work will also be presented.

## 1.2 LHC - A Multi Purpose Machine

The LHC is with a circumference of 27 km the largest hadron collider ever built. It uses superconducting magnets to create high magnetic fields to bend the particles carrying momenta of several TeV. Before they enter the LHC they are pre-accelerated by the LHC injector chain. The protons are first accelerated in Linac 2, Booster, Proton Synchrotron (PS) and Super Proton Synchrotron (SPS) [5] before they are injected into the LHC with an energy of 450 GeV. After the LHC is filled with the appropriate number of bunches, maximum 1380 in 2012 [6], the energy is ramped up to 4 TeV per beam (6-7 TeV beyond 2015). The beam sizes at Interaction Point (IP)s are then squeezed in order to deliver maximum number of collisions to the experiments. After the squeeze the particles are brought to collision at the 4 different IP, indicated in figure 1.1. There are 4 main detectors at the LHC. ATLAS and CMS are general purpose detectors with the main focus to explore new heavy particles [7, 8]. LHC beauty (LHCb) is studying the asymmetries between matter and anti-matter [9]. A Large Ion Collider Experiment (ALICE) is aimed to detailed studies of the heavy-ion collisions [10] during dedicated runs when the LHC instead of protons are filled with lead ions. This creates a higher energy density during the collisions, which enables the study of quark-gluon plasma. In the beginning of 2013 there was also a run colliding lead against protons [11]. There are also smaller experiments at the LHC. The Total elastic and diffractive cross-section measurement (TOTEM) detectors observe collisions at the same IP as the CMS detector but they are distributed up to 220 m away from the collision point [12]. A similar experiment: Absolute Luminosity For Experiment (ALFA) [13], is located at the same IP as ATLAS. Both ALFA and TOTEM are interested in observing the particles emitted in the very forward direction in order to measure the inelastic cross section of the protons as well as providing a luminosity monitoring for the two experiments. These experiments also have dedicated runs.

The different experiments can handle different rates of collisions. As a

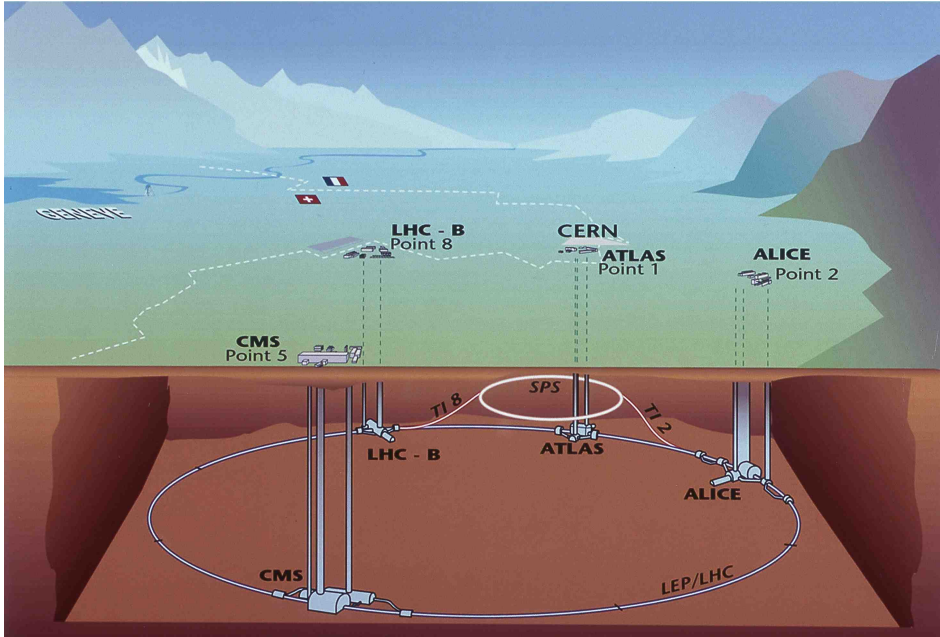


Figure 1.1: A conceptual drawing of LHC with the 4 main experiments.

consequence the beam is squeezed more for the general purpose experiments and less for LHCb and ALICE. The different modes of operation also change the request from the experiments. For example in case of the dedicated run for ALFA and TOTEM the beam is un-squeezed at those IPs. This flexibility of different modes of operation largely extends the physics potential of the LHC but adds extra efforts and complexity from the machine point of view. An example of such extra effort is that the different modes need different optics which have to be tested and corrected before they can be used in a physics run.

### 1.3 Hadron and Lepton Colliders: A Love Story

The development in particle physics has historically been driven by a mixture of hadron and lepton accelerators. The two types of accelerators have both provided crucial and complementary information to the particle physicists [14]. An example of this counter play was the discovery of the  $W^-$  and  $Z$ -bosons in 1983 with SPS<sup>1</sup>, for which Carlo Rubbia and Simon van der Meer were awarded the Nobel Prize in 1984 [15]. The  $W^-$  and  $Z$ -bosons were later very precisely measured in LEP. The measurement decreased the experimental uncertainty on a number of parameters important for the standard model. Most notably it was the precise measurement of the  $Z$ -boson that showed that there are 3 families of light neutrinos with a 98% confidence level [16].

<sup>1</sup>At the time of the discovery it was called  $S\bar{p}\bar{p}S$  since it was colliding protons with anti-protons.

### 1.3. Hadron and Lepton Colliders: A Love Story

---

What is actually the difference between leptons and hadrons in accelerators and particle physics? Leptons are, at the energies probed to date, fundamental particles, meaning that they do not have an inner structure. The hadrons on the other hand are composed of quarks and gluons and their momenta are distributed between them. The momenta of the individual quarks and gluons (partons) are described by the parton density function. At high energies collisions are described as collisions of two partons, as illustrated in figure 1.2(a). As a consequence only the conservation of transverse momenta can be used to constrain the kinematic variables in the event reconstruction.

In the case of a lepton-lepton collider the energy is well defined because of the point-like nature of the leptons, illustrated in figure 1.2(b).

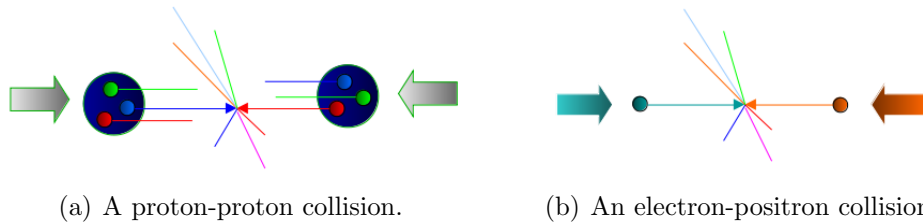


Figure 1.2: Collisions between different types of particles.

Additional benefits of colliding  $e^+$  and  $e^-$  instead of  $e^-$  and  $e^-$  is that the sum of the quantum numbers is zero after the collision. This enables direct production of new particles.

The electron and its anti-particle, the positron, are the only stable leptons with an electric charge. However, their low rest mass makes them irradiate substantial amount of synchrotron radiation when bent at high energies. The synchrotron radiation emitted each turn is given by the following formula [17]:

$$\Delta E = \frac{4\pi}{3} e^2 \beta^3 \frac{E^4}{rm^4} \quad , \quad (1.1)$$

where  $E$  is the total energy of the particle,  $e$  the electric charge,  $m$  is the mass of the particle,  $r$  is the radius and  $\beta$  is the relativistic factor. At LEP, which had a circumference of 27 km and an energy of 105 GeV per particle, the  $e^-$  and  $e^+$  lost almost 3% of their energy each turn to synchrotron radiation [18]. Since the synchrotron radiation scales with the fourth power, while the radius only scales inversely, it is clear that a bigger ring would only marginally decrease the synchrotron radiation. In contrast, the mass of the proton is 1836 times greater than the mass of the electron and therefore they emit  $\sim 10^{13}$  less synchrotron radiation for the same energy. Instead the limiting factors for the hadron machines, in the energy frontier, are the achievable magnetic fields and the total radius of the machine. In order to avoid the synchrotron radiation, a machine where the high energetic particles are not bent is needed. That is

why it is beneficial for the next high-energy  $e^+$  and  $e^-$  collider to be a linear collider.

## 1.4 Which Future Machine?

The motivation to build a lepton collider is driven by the possibility of precise measurements of particles like the newly discovered Higgs boson. The discussion is restricted to future possible high-energy lepton-colliders. The projects are competing with other facilities like neutrino factories, the high-energy LHC and the FCC-pp (Future Circular Collider proton-proton), but this is outside the scope of this discussion.

**CLIC** would be a linear  $e^+e^-$  collider with a possible energy reach of 3 TeV. It would use normal conducting accelerating structures to achieve accelerating gradient of 100 MV/m. It will use another beam to deliver the required RF power [19]. The CLIC concept is discussed in detail in chapter 6.

**ILC** (International Linear Collider) is a proposed 31 km linear  $e^+e^-$  collider utilising superconducting RF-structures to accelerate the particles to a center of mass energy of 500 GeV, with a possible upgrade to 1 TeV [20].

**FCC-ee** (Future Circular Collider  $e^+e^-$ ) is a proposed 80-100 km circular accelerator. The magnets would be normal conducting and it would collide  $e^+$  and  $e^-$ . The energy would be sufficient to produce both Higgs particles and top quarks. The advocates of this idea point out that the tunnel could later be reused for a hadron machine in the same way the LHC reused the LEP tunnel [21].

### Which machine is suitable for which scenario?

#### 1. Only the Higgs particle is discovered.

This would be a strong indication for a low energy linear collider. FCC-ee could also be a viable option, but a full cost review is still to be done for this project.

#### 2. New physics, like supersymmetry are discovered, in the range 0.5 TeV-1 TeV.

This scenario is looking more and more unlikely as the LHC is exploring more and more of this mass range for new particles [22]. However, in such scenario the ILC or a low energy CLIC would be two good options to perform precise measurements of the new particles.

#### 3. New physics above 1 TeV.

Such a scenario would be very favourable for CLIC. CLIC could then be built in two stages, starting with low energies to probe the Higgs particle and then

#### 1.4. Which Future Machine?

---

upgrade it to explore the energy of interest.

As important as the physics motivation for a future collider is the feasibility demonstration of the accelerator. It has to be shown without any doubt that the machine chosen is able to fulfill the requirements. Since the time scale of these projects is so long it is necessary to start the research and development well in advance. The predicted performance coming out of the studies for the different projects will also be a very important input in the process of deciding which machine to build. Chapter 7 describes the achievements done at CTF3 with focus on the improved beam stability. In doing so it also tries to play a role in the demonstration of the CLIC concept and hence in the decision of a future collider.



# Chapter 2

## Introduction to Beam Physics

In this chapter an introduction to beam physics is given. It focuses on the conceptual description of the parameters that govern the beam motion in an accelerator. The description is kept short and references are included for further reading.

### 2.1 Introduction

The main building blocks in an accelerator are the dipoles to steer the beam and the quadrupoles to focus it. In accelerator physics it is common to use the Frenet-Serret coordinate system, shown in figure 2.1 [23]. This coordinate system follows the reference path of the beam. The longitudinal position is denoted as  $s$ , the horizontal position is denoted as  $x$  and the vertical as  $y$ .

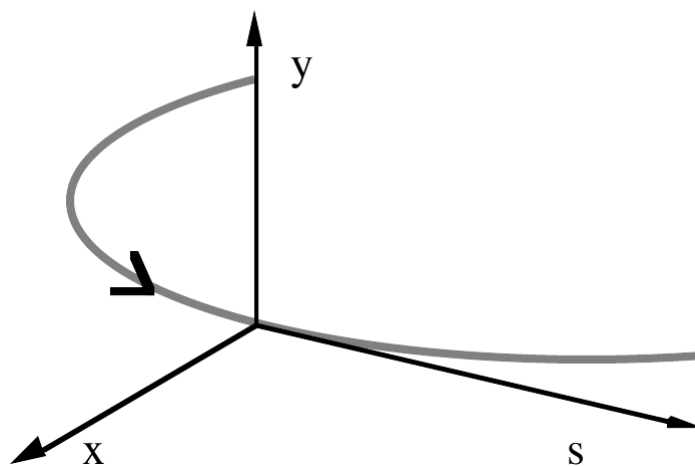


Figure 2.1: The Frenet-Serret coordinate system.

The general differential equation for transverse linear uncoupled motion is

described by Hill's equation:

$$x''(s) + k(s)x(s) = 0 \quad , \quad (2.1)$$

where  $k$  describes the focusing forces acting on the beam and varies with  $s$ . A focusing quadrupole has a  $k > 0$ , a defocusing has a  $k < 0$  and a drift space has  $k = 0$ . According to the theorem of Floquet, the solution with periodic boundary conditions, can be written in the form [23]:

$$x(s) = A\sqrt{\beta(s)} \cos[\psi(s) - \psi_0] \quad , \quad (2.2)$$

where  $\psi(s) = \int_0^s \frac{ds}{\beta(s)}$  and  $A, \psi_0$  are constants to be determined from the initial conditions. This is a pseudo harmonic oscillator with varying amplitude  $\sqrt{\beta(s)}$ . The  $\psi(s)$  is referred to as the phase and  $\psi(s_1) - \psi(s_0)$  is referred to as the phase advance between location  $s_1$  and  $s_0$ .

The transfer through a linear element may be represented with a matrix while describing sextupoles and higher order, magnets a transfer map formalism is needed [24]. The matrix describing the transfer from one location to another is obtained through multiplying all the elements between as

$$M = M_N M_{N-1} \dots M_2 M_1 \quad , \quad (2.3)$$

where  $M_i$  are the individual linear elements. Figure 2.2 shows the magnetic field line for a quadrupole together with the forces acting on a positively charged particle moving in the direction into the paper. A quadrupole in this configuration will give a focusing effect in the vertical plane but a defocusing effect in the horizontal plane. In the thin lens approximation the transfer matrix of a quadrupole focusing in vertical is given by [25]

$$\begin{pmatrix} y(s_2) \\ y'(s_2) \end{pmatrix} = \begin{pmatrix} 1 & 0 \\ -\frac{1}{f} & 1 \end{pmatrix} \begin{pmatrix} y(s_1) \\ y'(s_1) \end{pmatrix} \quad , \quad (2.4)$$

where  $f$  is the focusing related to the strength of the quadrupole,  $y$  the position and  $y'$  is the angle of the particle. In the horizontal plane there will be a defocusing effect which in the thin lens approximation may be described as

$$\begin{pmatrix} x(s_2) \\ x'(s_2) \end{pmatrix} = \begin{pmatrix} 1 & 0 \\ \frac{1}{f} & 1 \end{pmatrix} \begin{pmatrix} x(s_1) \\ x'(s_1) \end{pmatrix} \quad . \quad (2.5)$$

In case the magnet in figure 2.2 is rotated by  $\frac{\pi}{2}$  it will instead give a focusing in the horizontal plane. Through alternating the two types of quadrupole a net focusing is achieved. This is the most fundamental concept to keep the beam focused in modern particle accelerators.

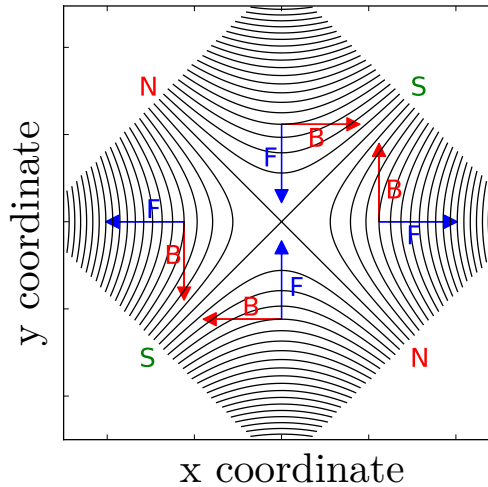


Figure 2.2: An illustration of a quadrupole.

## 2.2 Beam and Optics Parameters

### 2.2.1 Betatron Tune

The tune in an accelerator is the number of betatron oscillations over a full turn. It is related to the  $\beta$ -function as described by Eq. (2.6).

$$Q = \frac{1}{2\pi} \oint \frac{ds}{\beta(s)} \quad (2.6)$$

The tune is an important parameter to measure and control in a circular accelerator. It affects the dynamics of the beam motion and at certain values it leads to beam instabilities, further discussed in the next section.

### 2.2.2 Resonances

It is desired to keep the tune away from fractional values with small denominators such as  $\frac{1}{2}$ ,  $\frac{1}{3}$ . Exceptions to this are slow extraction using nonlinear resonances [26, 27]. The resonances occur when the perturbations act synchronous with the oscillations. If the tune approaches an integer the beam is exposed to the same perturbations every turn.

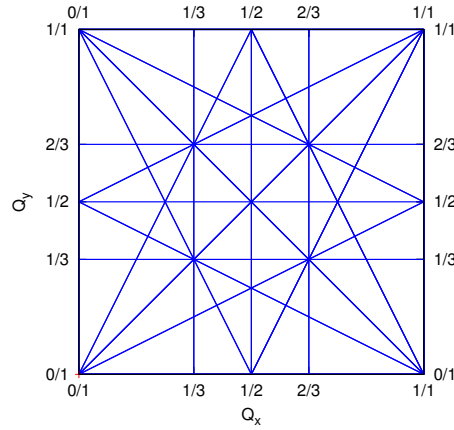
The resonance condition is given by Eq. (2.7). The order ( $n$ ) of a resonance is  $n = |a| + |b|$ , where  $a$  and  $b$  are as defined in Eq. (2.7).

$$aQ_x + bQ_y = p \quad \text{where } a, b, p \in \mathcal{Z} \quad (2.7)$$

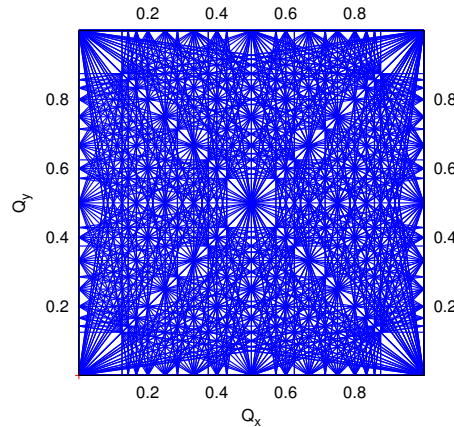
The width of a resonance in the tune space is termed the stopband. Most of the resonances drive the particles unstable through rapid increase in the amplitude of the oscillations. Example of unstable resonances includes  $2Q_{x,y} = p$

and the ( $Q_x + Q_y = p$ ). The difference coupling resonance ( $Q_x - Q_y = p$ ) is on the other hand inherently stable but may cause other unwanted effects further discussed in chapter 4.

Figure 2.3 shows the resonance diagram up to a certain order. The figures were generated through the use of Farey sequences [28, 29].



(a)  $n \leq 3$



(b)  $n \leq 8$

Figure 2.3: The resonance diagram defined in the tune space  $(Q_x, Q_y)$ .

### 2.2.3 $\beta$ -function

The  $\beta$ -function is a property of the lattice. In a circular machine it is fully determined by the layout and powering of the magnets. In case of large  $\beta$  the beam is less focused, hence occupying a larger transverse space compared to locations with small  $\beta$ .

It is common to define the beam envelope as

$$e(s) = \sqrt{\beta(s)}\epsilon \quad , \quad (2.8)$$

where  $\epsilon$  is the size of the phase space occupied by the particles, described in more detail in section 2.2.6. The beam envelope states the transverse space occupied by the beam for all different phase advances.

The relative deviation in  $\beta$ -function between the model and the measurement is referred to as  $\beta$ -beat ( $\frac{\beta_{model}-\beta_{meas}}{\beta_{model}}$ ).

The  $\beta^*$  is referring to the minimum  $\beta$ -function at the waist. In a collider the waist should be at the location where the particles collide.

### 2.2.4 Dispersion

Particles with different energies are bent differently. A particle with higher energy will be bent less compared to one with lower energy. This gives rise to dispersion which is defined as

$$D(s) = \frac{\Delta x(s)}{\Delta p/p} \quad , \quad (2.9)$$

where  $\Delta x(s)$  is the deviation from the reference orbit and  $\Delta p/p$  the relative momentum deviation.

### 2.2.5 Chromaticity

A quadrupole can be seen as a lens which focuses particles. However, particles with higher energy will be focused less compared to particles with lower energy. This is conceptually illustrated in figure 2.4. As a consequence the phase advance will be different for particles with different energy. This effect is termed chromaticity and for a circular machine it is defined as

$$Q' = \frac{\Delta Q}{\Delta p/p} \quad , \quad (2.10)$$

where  $\Delta Q$  is the tune change and  $\Delta p/p$  is the relative momentum deviation.

### 2.2.6 Emittance

Emittance is a beam parameter which describes the area the beam occupies in the phase space. According to Liouville's theorem the emittance remains constant under the influence of conservative forces [30]. For example it is not possible to reduce the emittance with magnets. This makes it a very important parameter to maintain. An increase of the emittance will mean that the beam is occupying a larger phase space which can cause beam losses and decrease the luminosity. In figure 2.5 the phase space ellipse is plotted. The ellipse is given by the following equation:

$$\gamma^2 x + 2\alpha x x' + \beta x'^2 = \epsilon \quad (2.11)$$

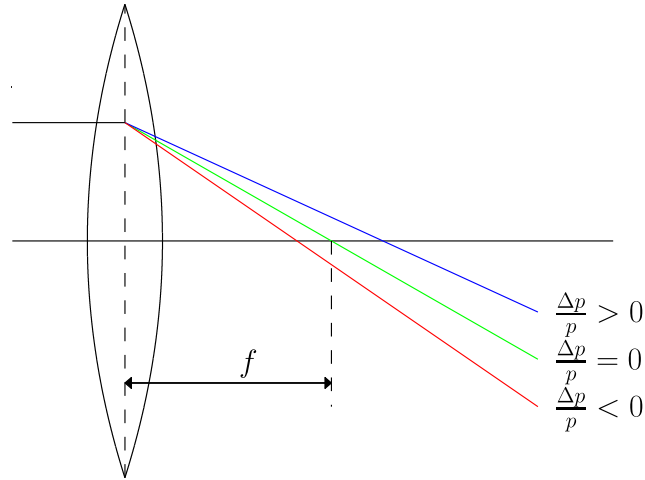


Figure 2.4: Illustration of the effect of chromaticity in a focusing quadrupole magnet. The particles with  $\Delta p/p > 0$  (blue line) are under-focused while the particles with  $\Delta p/p < 0$  (red line) are over-focused. Only the particles with  $\Delta p/p = 0$  (green line) are focused according to the design.

where  $\beta$  is the amplitude beta function,  $\alpha = -\frac{1}{2}\frac{\partial\beta}{\partial s}$  and  $\gamma = \frac{1+\alpha^2}{\beta}$ . These parameters are referred to as the Courant-Snyder parameters and are commonly used in accelerator physics [31].

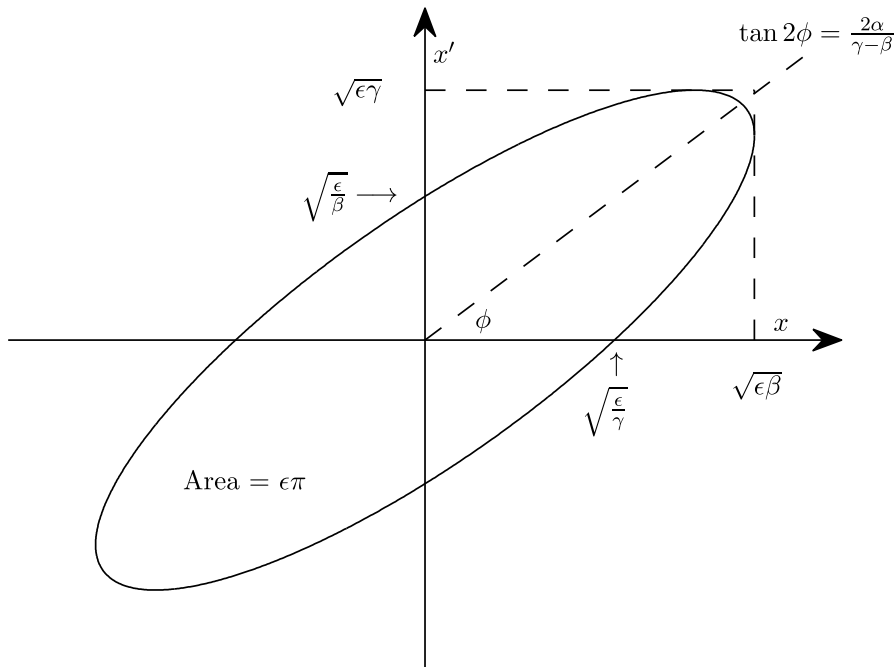


Figure 2.5: The phase space ellipse.

In figure 2.6 (a,b) the emittance for two different  $\beta$ -functions is plotted. In both cases  $\alpha = 0$  which corresponds to the situation at the IPs. The emittance

## 2.3. Decoherence

is the same for the two cases but due to the difference in  $\beta$  the transverse size is much larger for the 90 m compared to the 0.6 m case. Figure 2.6 (c,d) show the cross section of the beam and the arrows indicate the angle of the particles inside the beam in the transverse directions. The vertical emittance and  $\beta$  are assumed to be the same as the horizontal. As expected the beam size for the  $\beta = 90$  m is larger but the small arrows show that the angles of the particles are small. In the case of the  $\beta = 0.6$  m the situation is different. In this case the beam size is small but the particles have large angles. The green dots show the position of the particles. If the main interest is luminosity production a lower

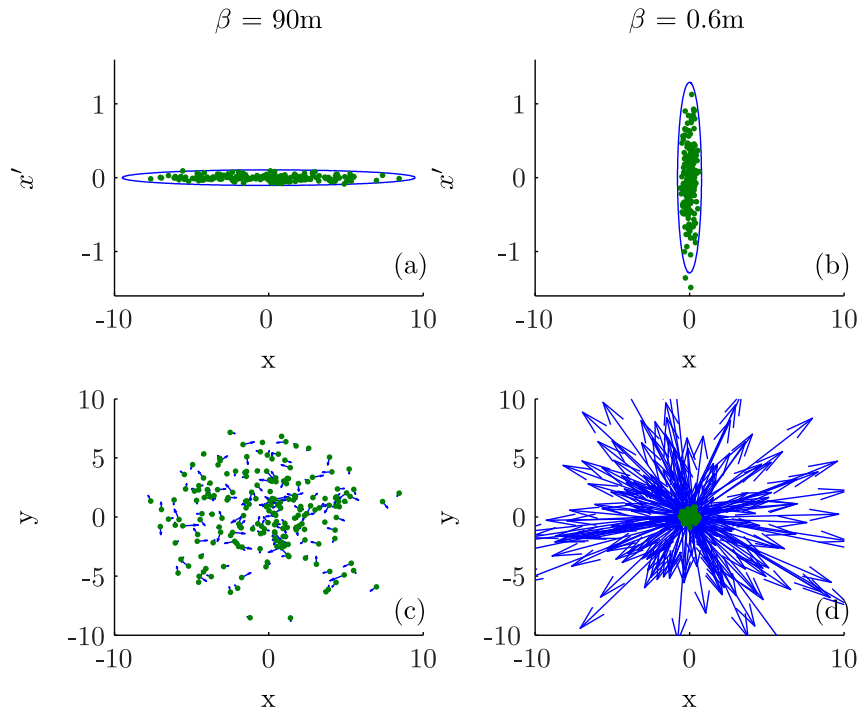


Figure 2.6: The phase space ellipse for  $\beta = 90$  m (a) and  $\beta = 0.6$  m (b) with the same emittance. The ellipse is chosen to contain particles up to  $3\sigma$ . The bottom plots show the cross section of the beam,  $\beta = 90$  m (c) and  $\beta = 0.6$  m (d). The angles are indicated with the blue arrows while the green dots show the position of the particles.

$\beta^*$  is preferred. In case it is important that the particles are moving parallel to the beam axis a larger  $\beta^*$  is required.

## 2.3 Decoherence

Decoherence is an effect that derives from a beam containing particles with different tunes. If the particles all have the same betatron tune, the observed centroid motion is harmonic. If the beam contains a spread of tunes, the motion will decohere as the particles' betatron phases disperse. As a consequence

the observed centroid of the beam will show a decaying oscillation. It should be stressed that this is not a damping of the individual particle's oscillation. Instead the individual particle will keep its amplitude oscillation but since they are at different transverse locations the observed oscillation will be averaged in the Beam Position Monitor (BPM). The two main sources for decoherence are [32]:

- Non linear transverse fields.
- Chromaticity in combination with energy spread of the beam.

Figure 2.7 shows the decoherence of a beam containing particles with different tunes. The upper plot in the figure shows the turn-by-turn data for particles with different tunes. The bottom plot shows the mean value, or what a BPM would measure. This is the situation in a machine with high chromaticity in combination with energy spread and no RF. In the presence of RF the particles will experience a restoring force and the high-energy particles will be slowed down and the low-energy particles will be accelerated more. In this way the particles will re-cohere after a full synchrotron period. However, in case of non-linearity the particles will not re-cohere and this makes it possible to distinguish the two effects [32].

## 2.4 Non-linear Magnetic Multipoles

Sextupolar fields and higher are termed non-linear magnetic fields. They are installed and serve important purposes in most accelerators. Unwanted higher order fields which derive from imperfections in lower order magnets can, however, if not corrected cause significant disturbance for the beam. The order of a multipole is commonly labeled  $n$ , where  $n = 1$  is a dipole,  $n = 2$  is a quadrupole,  $n = 3$  a sextupole, etc. The magnetic field of the multipole is given by Eq. (2.12).

$$B_y(x,y,s) + iB_x(s,y,s) = [B_n(s) + iA_n(s)] (x + iy)^{n-1} \quad (2.12)$$

$B_n(s)$  and  $A_n(s)$  are the respective normal and skew multipole coefficients, defined in Eq. (2.13) and Eq. (2.14). A skew multipole is a normal multipole rotated by  $\frac{\pi}{2n}$ , which means that a skew quadrupole is rotated with  $\frac{\pi}{4}$  compared to a normal quadrupole.

$$B_n(s) = \frac{1}{(n-1)!} \left. \frac{\partial^{n-1} B_y}{\partial x^{n-1}} \right|_{(0,0,s)} \quad (2.13)$$

$$A_n(s) = \frac{1}{(n-1)!} \left. \frac{\partial^{n-1} B_x}{\partial x^{n-1}} \right|_{(0,0,s)} \quad (2.14)$$

In the linear approximation the Hamiltonian may be written as

$$\mathbf{H}_0 = \frac{1}{2}p_x^2 + \frac{1}{2}p_y^2 + \frac{1}{2}K(\theta)x^2 - \frac{1}{2}K(\theta)y^2 \quad , \quad (2.15)$$

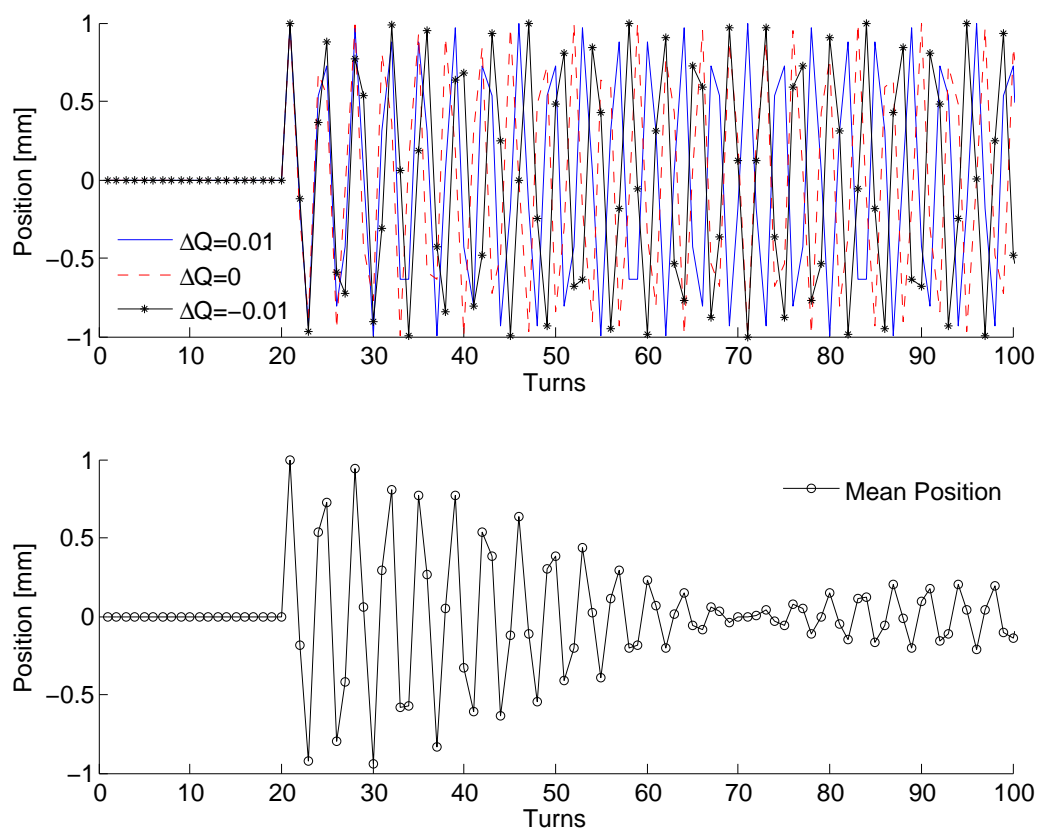


Figure 2.7: A conceptual figure of decoherence. The beam is kicked at turn 20. At this point the particles have the same phase but later they start to decohere. The upper plot shows 3 individual particles with different tunes. The lower plot shows the mean position of the particles, which is what is observed by the BPMs.

where  $K(\theta)$  describes the variation of focusing strength around the ring.

Higher order fields are usually described as a perturbation to the linear Hamiltonian. The contribution to the Hamiltonian of a multipole of order  $n$  is given by

$$\mathbf{H}_n = \frac{q}{p} \operatorname{Re} \left[ \frac{1}{n} [B_n(s) + iA_n(s)] (x + iy)^n \right] , \quad (2.16)$$

where  $q$  is the charge of the particle and  $p$  is the momentum. If the Hamiltonian for an  $n^{\text{th}}$  order normal multipole is labeled  $N_n$ , and the Hamiltonian for an  $n^{\text{th}}$  order skew multipole denoted  $S_n$ , then

$$N_n \propto \operatorname{Re} [(x + iy)^n] \quad S_n \propto \operatorname{Im} [(x + iy)^n] . \quad (2.17)$$

## 2.5 Coupling

When the motion in the transverse planes are independent the motion is said to be uncoupled. This is normally the preferred behaviour in a collider such as the LHC. There are a several different effects that may act to couple the motion in an accelerator. The main sources of linear coupling are solenoids and skew quadrupole fields. An example of a skew quadrupole is shown in figure 2.8.

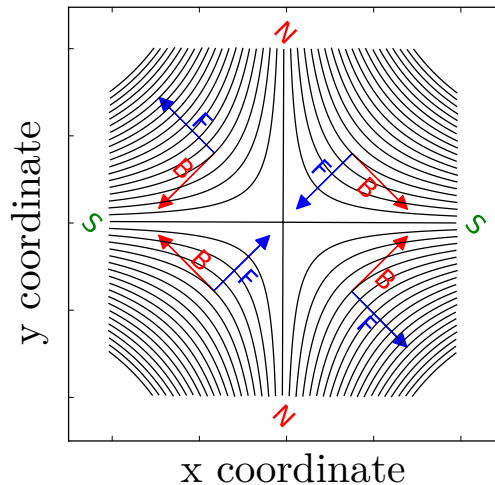


Figure 2.8: An illustration of a skew quadrupole.

### 2.5.1 Parametrization of Linear Coupling

There exist different ways to parametrize coupled beam motion in an accelerator. The two most commonly used are Edwards-Teng [33] and Mais-Ripken [34] parametrization.

## 2.6. Resonance Driving Terms

---

Since the coupling by definition introduces a dependency between the horizontal and vertical plane, the motion can no longer be described by two independent  $2 \times 2$  matrices. Instead it has to be described by a  $4 \times 4$ , such as

$$\hat{\mathbf{M}} = \begin{pmatrix} \mathbf{P} & \mathbf{p} \\ \mathbf{q} & \mathbf{Q} \end{pmatrix}, \quad (2.18)$$

where  $\mathbf{P}$ ,  $\mathbf{p}$ ,  $\mathbf{q}$  and  $\mathbf{Q}$  are  $2 \times 2$  matrices. When the motion is uncoupled the matrices  $\mathbf{p}$  and  $\mathbf{q}$  are 0.

In the Edwards-Teng parametrization, described in [33], the linear coupling is described by a symplectic rotation  $\mathbf{R}$  of  $\hat{\mathbf{M}}$  into its normal modes form  $\bar{\mathbf{M}}$ , described by Eq. (2.19). In this frame the motion is decoupled.

$$\bar{\mathbf{M}} = \begin{pmatrix} \mathbf{X} & 0 \\ 0 & \mathbf{Y} \end{pmatrix} = \mathbf{R}\hat{\mathbf{M}}\mathbf{R}^{-1} \quad (2.19)$$

Edwards and Teng characterized the transformation  $\mathbf{R}$  by the symplectic matrix:

$$\begin{pmatrix} \mathbf{I} \cos \theta & -\mathbf{K}^{-1} \sin \theta \\ \mathbf{K} \sin \theta & \mathbf{I} \cos \theta \end{pmatrix}, \quad (2.20)$$

where  $\mathbf{I}$  is the  $2 \times 2$  unit matrix, and  $\mathbf{K}$  is a  $2 \times 2$  symplectic matrix:  $\det(\mathbf{K}) = 1$ . The situation may then be described by the uncoupled Twiss parameter, together with the elements of matrix  $\mathbf{K}$  and Teng's angle of rotation  $\theta$ . In case the angle  $\theta = 0$  the matrix  $\mathbf{R}$  is the identity matrix and as a result it will not rotate any of the modes.

## 2.6 Resonance Driving Terms

The theory of Resonance Driving Term (RDT) provides an important tool in studies of coupling and nonlinear sources. In this section an introduction to the resonance driving terms will be given and in appendix A a derivation of the driving terms up to first order is given. A discussion on the use of RDTs to measure coupling is also presented.

The evolution of the horizontal variable, in the resonance basis, as a function of the turn number  $N$  is given by

$$h_x^-(N) = \sqrt{2I_x} e^{i(2\pi\nu_x N - \psi_{x0})} - 2i \sum_{jklm} j f_{jklm} (2I_x)^{\frac{j+k-1}{2}} (2I_y)^{\frac{l+m}{2}} e^{i[(1-j+k)(2\pi\nu_x N - \psi_{x0}) + (m-l)(2\pi\nu_y N - \psi_{y0})]}, \quad (2.21)$$

and for the vertical plane by

$$h_y^-(N) = \sqrt{2I_y} e^{i(2\pi\nu_y N - \psi_{y0})} - 2i \sum_{jklm} l f_{jklm} (2I_x)^{\frac{j+k}{2}} (2I_y)^{\frac{l+m-1}{2}} e^{i[(k-j)(2\pi\nu_x N - \psi_{x0}) + (1-l+m)(2\pi\nu_y N - \psi_{y0})]} \quad , \quad (2.22)$$

where  $I$  is the action,  $\phi$  is the phase of the action-angle variable,  $f_{jklm}$  is the resonance driving terms and  $\nu$  is the perturbed tunes. A multipole of order  $n$  is related to a term in the Hamiltonian  $x^{j+k}y^{l+m}$  where  $n = j + k + l + m$ .

The term in  $e^{i[(k-j)(2\pi\nu_x N - \psi_{x0}) + (1-l+m)(2\pi\nu_y N - \psi_{y0})]}$  shows that the different terms will give rise to modes in the beam motion with different frequency. For example when  $j = m = 1$  the second term in Eq. (2.21) becomes:  $-2i f_{1001} \sqrt{2I_y} e^{2\pi\nu_y N - \phi_{y0}}$ . From this we observe that the  $f_{1001}$  will give rise to a peak in the horizontal spectrum at the frequency of the vertical tune. More generally, it is observed that each term in the expansion corresponds to a mode in the beam motion and hence contributes to a certain frequency of the motion. Note, however, that if  $l = j = 0$  then the second term will be zero and hence not contribute to any motion. The relation between the amplitude of the RDTs and the amplitude of the peaks is described as

$$\begin{aligned} H(1-j+k, m-l) &= 2j |f_{jklm}| (2I_x)^{\frac{j+k-1}{2}} (2I_y)^{\frac{l+m}{2}} \\ V(k-j, 1-l+m) &= 2l |f_{jklm}| (2I_x)^{\frac{j+k}{2}} (2I_y)^{\frac{l+m-1}{2}} \quad . \end{aligned} \quad (2.23)$$

The different  $f_{jklm}$  drive different resonances. This is described in Eq. (2.24).

$$(j-k)Q_x + (l-m)Q_y = p \quad \text{where } p \in \mathcal{Z} \quad (2.24)$$

In case of the  $f_{1001}$  this will drive the resonance  $Q_x - Q_y = p$ . The  $f_{1001}$  and  $f_{0110}$  describe the same dynamics but  $f_{1001}$  is for the horizontal plane while  $f_{0110}$  is for the vertical plane. Since they describe the same dynamics it is custom to label both of them as  $f_{1001}$ . This notation has been adopted throughout the thesis.

The amplitude of the  $|f_{1001}|$  may be obtained from the Fourier spectrum of the turn-by-turn (TbT) data. Using Eq. (2.24) for  $j = 1, m = 1$  we obtain  $H(0,1) = |f_{1001}| (2I_y)^{\frac{1}{2}}$ . In order to calculate the  $f_{1001}$  independent of the action we divide with  $2V(0,1) = 2\sqrt{2I_y}$  which gives us the relation  $|f_{1001}| = \frac{H(0,1)}{2V(0,1)}$ .

In order to construct the  $h_z^-$  from TbT data position and transverse momentum are required. In case only the position data is used the spectral analysis will mix lines  $Z(a,b)$  with  $Z(-a, -b)$ . This is the case for example for the  $f_{1001}$  and  $f_{1010}$  which are not separable from only the position data. A more detailed discussion on this is given in chapter 4.

# Chapter 3

## Optics Corrections in the LHC

The LHC requires good control of the optics functions. The control of the  $\beta$ -functions is essential for safe beam operation [35] due to the destructive power of the LHC beams. A larger deviation from the model of the injection optics also causes an increased emittance and hence a decrease in luminosity. A good control of the  $\beta^*$  is essential to ensure the requested luminosity. This chapter will describe the measurements and corrections of the LHC optics. First, the methods will be described, followed by the procedure of a measurement and correction. Finally, the results from the corrections of the nominal and the high- $\beta^*$  optics will be shown.

### 3.1 Optics Measurements Methods

#### 3.1.1 Exciting the Beam

In order to measure the optics an oscillation around the closed orbit is induced. It is necessary to have a big enough oscillation so it can be recorded by the BPMs. In storage rings this is traditionally done with a kicker. The BPMs measure the position of the beam on a turn-by-turn basis. By performing a spectral analysis of the data it is possible to reconstruct the optics. However, after the beam is kicked it will decohere, which will cause an emittance increase. As a consequence, a beam can only be kicked a few times before a new one needs to be injected. After a beam is dumped in the LHC, it can take several hours to reach the same machine setting again. The machine has to be pre-cycled, the beam has to be injected, then the energy has to be ramped and the  $\beta^*$  has to be squeezed. As a consequence using a normal kick is not the optimal solution. Instead an AC-Dipole is used to excite the beam. The AC-dipole is a fast oscillating magnet, which can be adiabatically turned on and off [36]. In this way it creates coherent oscillations of the beam particles without affecting the transverse emittance. The use of the AC-dipole also introduces systematic

effects on the optics measurements. The methods to correct those systematic effects are described in detail in [37, 38].

### 3.1.2 Measuring the Phase

In order to measure the phase of the oscillations a Fourier Transform (FT) is performed to the data. In practice this was done with a modified version of the SUSSIX code [39]. The SUSSIX code performs an interpolated FT. The assumption is that the form of the spectrum is known and that it corresponds to a pure sinusoidal. Using this method the tune resolution of the measurement can be improved [25]. For a perfect sinusoidal the resolution should scale as  $\frac{1}{N^2}$  compared to a  $\frac{1}{N}$  for a normal FT, where N is the number of turns.

### 3.1.3 Measuring the $\beta$ -function

It is possible to calculate the  $\beta$ -function using the phase advance from 3 BPMs together with the local model between them. With this method the  $\beta$ -function can be determined without influence of the calibration of the BPMs but it relies on a good local model. In case e.g. a quadrupole is wrongly placed relative to the local model this method will give an incorrect  $\beta$ -function at the BPM. The equation to calculate the  $\beta$ -function is the following [25]

$$\beta_1 = \left( \frac{1}{\tan \phi_{21}} - \frac{1}{\tan \phi_{31}} \right) / \left( \frac{m_{11}}{m_{12}} - \frac{n_{11}}{n_{12}} \right) \quad , \quad (3.1)$$

where  $\phi_{ij}$  is the phase advance from BPM  $i$  to  $j$ ,  $m_{ij}$  is the matrix element in the matrix  $\mathbf{M}(1 \rightarrow 2)$  and  $n_{ij}$  is the matrix element in the matrix  $\mathbf{N}(1 \rightarrow 3)$ . However, for calculating the corrections we do not rely on the local model but instead we correct the phase. It was shown in [40] that the correction of the phase advance has the same effect as correcting the actual  $\beta$ -function. The benefit is that measuring the phase advance between two BPMs is both model and calibration independent. For these reasons the phase-beating between consecutive BPMs is chosen as the observable to minimize, which is given by

$$\Delta\phi_i = \phi_i^{meas} - \phi_{i-1}^{meas} - (\phi_i^{mod} - \phi_{i-1}^{mod}) \quad , \quad (3.2)$$

where  $i$  is the BPM index and the superscript refers to if it is a measurement or the model.

### 3.1.4 K-modulation

It is possible to calculate the  $\beta$ -function at a quadrupole through changing the magnetic fields in it while measuring the change in tune. This method has been used to measure the  $\beta^*$  for different optics in the LHC. In this case the  $\beta$ -function is measured at the magnets closest to the IP and the  $\beta$  is propagated from both sides to get the  $\beta^*$  [41]. The tune is measured with the

diode-based base-band-tune (BBQ)-system, which provides a precise tune measurement without any additional beam excitation [42].

The transfer matrix describing the evolution for one turn may be written as [25]

$$\begin{pmatrix} \cos(2\pi Q_{x,y}) + \alpha_{x,y} \sin(2\pi Q_{x,y}) & \beta_{x,y} \sin(2\pi Q_{x,y}) \\ -\sin(2\pi Q_{x,y}) & \cos(2\pi Q_{x,y}) - \alpha_{x,y} \sin(2\pi Q_{x,y}) \end{pmatrix} . \quad (3.3)$$

The change in integrated gradient of the quadrupole can be represented as a deflection [25]:

$$\Delta x' = -Kx \quad , \quad (3.4)$$

where  $K$  is the integrated quadrupole strength. The kick may be represented as a perturbation matrix:

$$\begin{pmatrix} 1 & 0 \\ \pm(\Delta K) & 1 \end{pmatrix} . \quad (3.5)$$

Next step is to relate the tune difference to the change in the quadrupole. The right hand side of the equation is obtained by multiplying the perturbation matrix with the turn-by-turn and calculating the trace of it. The left side is obtained by taking the trace of the transport matrix with the new tune  $Q_{x,y} + \Delta Q_{x,y}$ . This gives

$$2 \cos(2\pi(Q_{x,y} + \Delta Q_{x,y})) = 2 \cos(2\pi(Q_{x,y})) - \beta_{x,y}(\pm(\Delta K) \sin(2\pi Q_{x,y})) \quad . \quad (3.6)$$

Since the  $\Delta K$  and the tune are known it is possible to solve for  $\beta_{x,y}$ , which gives

$$\beta_{x,y} = \pm \frac{2}{\Delta K} [\cot(2\pi Q_{x,y})(1 - \cos(2\pi \Delta Q_{x,y})) + \sin(2\pi \Delta Q_{x,y})] \quad , \quad (3.7)$$

where  $\Delta Q_{x,y}$  is the change in tune. If the change in tune is small and far from the integer and half integer resonances  $\beta_{x,y}$  can be approximated as

$$\beta_{x,y} \approx \pm 4\pi \frac{\Delta Q_{x,y}}{\Delta K} \quad . \quad (3.8)$$

#### 3.1.5 Measuring Dispersion

Through adjusting the RF-frequency it is possible to adjust the energy of the beams slightly. The mean orbit is recorded for the different energies and the dispersion is calculated for each individual BPM as

$$D_x = \frac{\Delta x}{\Delta p/p} \quad . \quad (3.9)$$

The measurement of the normalized dispersion  $\frac{D}{\sqrt{\beta}}$  is more robust since it is independent of the BPM calibration and the model [43]. The quantity becomes independent since both the dispersion- and the  $\beta$ -function measurements dependencies cancel out.

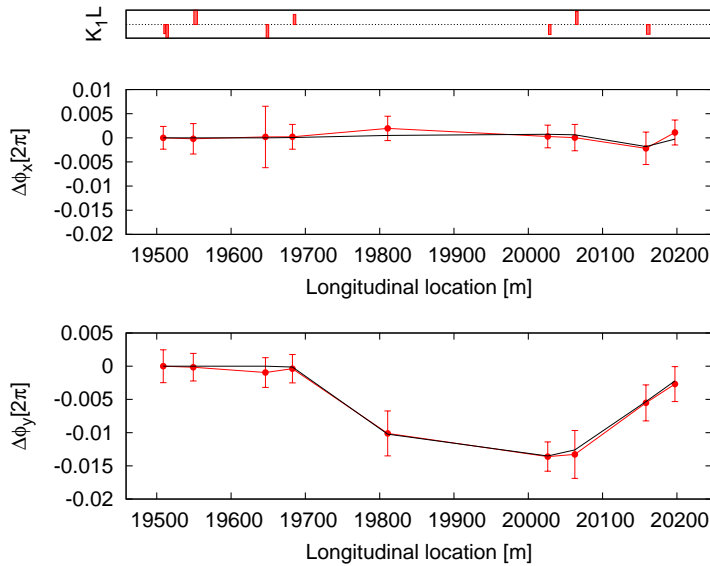


Figure 3.1: An example of a local correction. The red error bars represent the measurement and the black line is the model with introduced errors.

## 3.2 Correction Methods

The optics corrections in the LHC are based on two different methods. The global correction minimizes the errors globally. The local correction technique is developed to correct local sources and is mostly used around the IPs.

### 3.2.1 Local Corrections

The idea with local corrections is to treat one part of the accelerator as a line. The method was designed and used to find and correct errors locally [44]. First, the segment of interest is chosen. The optics parameters are taken from the model and propagated and compared to the measurements. Corrections are applied to individually powered magnets in order to reproduce the measurements. The corrections found are then applied to the magnets in the machine but with the opposite sign.

The parameter to minimize for the phase advance is:

$$\Delta\phi_{error} = \phi_{model} - \phi_{measurement} \quad . \quad (3.10)$$

An example of a local correction of the phase advance around IP6 is shown in figure 3.1. Note that the plotted phase advance is the deviation from the ideal model.

#### 3.2.2 Global Corrections

The global correction algorithm is based on a matrix inversion approach. The response matrix  $\mathbf{R}$  is created using the ideal model MADX (Methodical Accelerator Design) [45]. The matrix relates the optics functions at the BPMs with the change of the quadrupoles [44]. The relation can be described as

$$\mathbf{R}\Delta\vec{K} = (\Delta\vec{\phi}_x, \Delta\vec{\phi}_y, \Delta\frac{\overrightarrow{D_x}}{\sqrt{\beta_x}}, \Delta Q_x, \Delta Q_y) \quad . \quad (3.11)$$

To calculate a correction the inverted matrix,  $\mathbf{R}^{-1}$  is multiplied with the measurement. The system is over constrained but solvable in the least squares sense. It is also possible to weight the importance of parameters differently or ignore one completely. The inversion of the matrix can be described as:

$$\Delta\vec{K} = \mathbf{R}^{-1}(w_1\Delta\vec{\phi}_x, w_2\Delta\vec{\phi}_y, w_3\Delta\frac{\overrightarrow{D_x}}{\sqrt{\beta_x}}, w_4\Delta Q_x, w_5\Delta Q_y) \quad , \quad (3.12)$$

where  $w_i$  are adjustable parameters which change the emphasis of the correction.

### 3.3 Correction Procedure

For safety reasons the optics studies in the LHC are conducted with pilot bunches. These bunches have lower intensity than bunches used for collisions. The intensity for pilots bunches is chosen such that they should not cause any major damages if lost but still provide a sufficient signal for the BPMs. It is predicted that they could, if lost at the wrong place, induce a quench of a magnet. A quench could in worst case result in days of down time and should therefore be avoided. The following points explain the procedure used to correct the optics in LHC.

1. A bunch is injected, accelerated and the optics is adjusted to the one of interest.
2. The collimators are then moved further away from the beam to increase the aperture for the excitation of the beam.
3. The beam is excited by the AC-Dipole. It is first excited with a low amplitude. If the losses are too high the beam will automatically be dumped by the Beam Loss Monitoring system. The losses also decrease the beam intensity. In case a too large fraction of the beam is lost it is not longer possible to use it for accurate measurements. When an appropriate kick amplitude is found the beam is excited a few times to reduce the statistical errors.
4. The measured data is then processed in a set of computer codes to reconstruct the optics functions. The results are displayed in a Graphical

User Interface (GUI) together with the expectations from the model [46]. If the  $\beta$ -beat is larger than  $\sim 40\%$  a local correction is needed. If not we go straight to point 7.

5. It can be time consuming to find local corrections. If possible, other measurements or optimizations can be done while the local corrections are calculated.
6. After the local corrections have been applied a remeasurement of the optics is performed.
7. The global correction is calculated as described in section 3.2.2. The time consumption to calculate the global correction is small so it is normally calculated and applied during the same shift.
8. After the corrections have been applied a measurement is performed to validate that the corrections were successful.

## 3.4 Results

The results presented in this section reflect contributions from all the members of the Optics Measurement and Correction (OMC) team. The author played an important role in all the measurements and corrections presented and a leading role during the commissioning of the high- $\beta$  optics.

### 3.4.1 Nominal Optics

In the beginning of 2012 a full recommissioning of the optics was done. All the corrections calculated for the previous run were removed and the virgin machine was measured. Using this approach an unprecedented low  $\beta$ -beat for a hadron collider was achieved. The procedure and the results are presented in details in Paper I.

### 3.4.2 High $\beta^*$

The main motivation to un-squeeze the beam is to minimize the angles the particle collide with. In case of large  $\beta^*$  the two beams are moving towards the IP more parallel to the beam line resulting in less angle for the colliding particles. This effect is shown in figure 2.6(c).

The different optics are referred to by their  $\beta^*$  at IP1 and IP5. The other IPs remained unchanged with injection settings.

#### 3.4.2.1 $\beta^* = 90$ m

Already in 2011 there was a dedicated run for the TOTEM and ALFA experiments where the optics was un-squeezed to 90 m [47]. In 2012 the optics was remeasured with the same corrections as in 2011. The  $\beta$ -beat for the two measurements is shown in figure 3.3. It is remarkable that the corrections have

### 3.4. Results

---

Table 3.1: The weighted mean value of the normalized dispersion deviation from the model for  $\beta^* = 1000$  m, before and after correction, for Beam 1 and Beam 2 respectively.

	$\left\langle \frac{D_x}{\sqrt{\beta_x}} \right\rangle$	$\left\langle \frac{D_x}{\sqrt{\beta_x}} \right\rangle$
	Before Correction [ $\text{m}^{-1/2}$ ]	After Correction [ $\text{m}^{-1/2}$ ]
Beam 1	$9.5 \times 10^{-3}$	$4.1 \times 10^{-3}$
Beam 2	$8.5 \times 10^{-3}$	$4.0 \times 10^{-3}$

remained valid over this time period. This shows the good reproducibility of the LHC optics. Since the optics was already corrected to a good level, no new corrections were calculated in 2012 for the 90 m optics.

#### 3.4.2.2 $\beta^* = 500$ m

The correction of the 500 m optics was done after first removing the corrections for the 90 m. First the un-corrected machine was measured, see figure 3.3. For Beam 2 a local correction was performed, prior to the global correction, but due to technical problems this step was skipped for Beam 1. The final results after global correction for Beam 1 and Beam 2 are both below 10%  $\beta$ -beat.

#### 3.4.2.3 $\beta^* = 1000$ m

After a successful physics run at  $\beta^* = 500$  m it was decided to try to un-squeeze the beam further. It was observed during the 500 m optics commissioning that local corrections did not significantly improve the results when the  $\beta$ -beat was already in the level of  $\sim 30\%$ . As a consequence no local corrections were calculated for the 1000 m optics. At this optics off-momentum measurements were taken in order to calculate the dispersion. The normalized dispersion and the phase advance were corrected simultaneously. In figure 3.4 a comparison of the normalized dispersion before and after the correction is shown. The weighted mean value of the normalized horizontal dispersion is presented in table 3.1. The dispersion beating was reduced roughly by a factor 2 for both beams. The  $\beta$ -beat is presented in Paper II together with the results from the K-modulation.

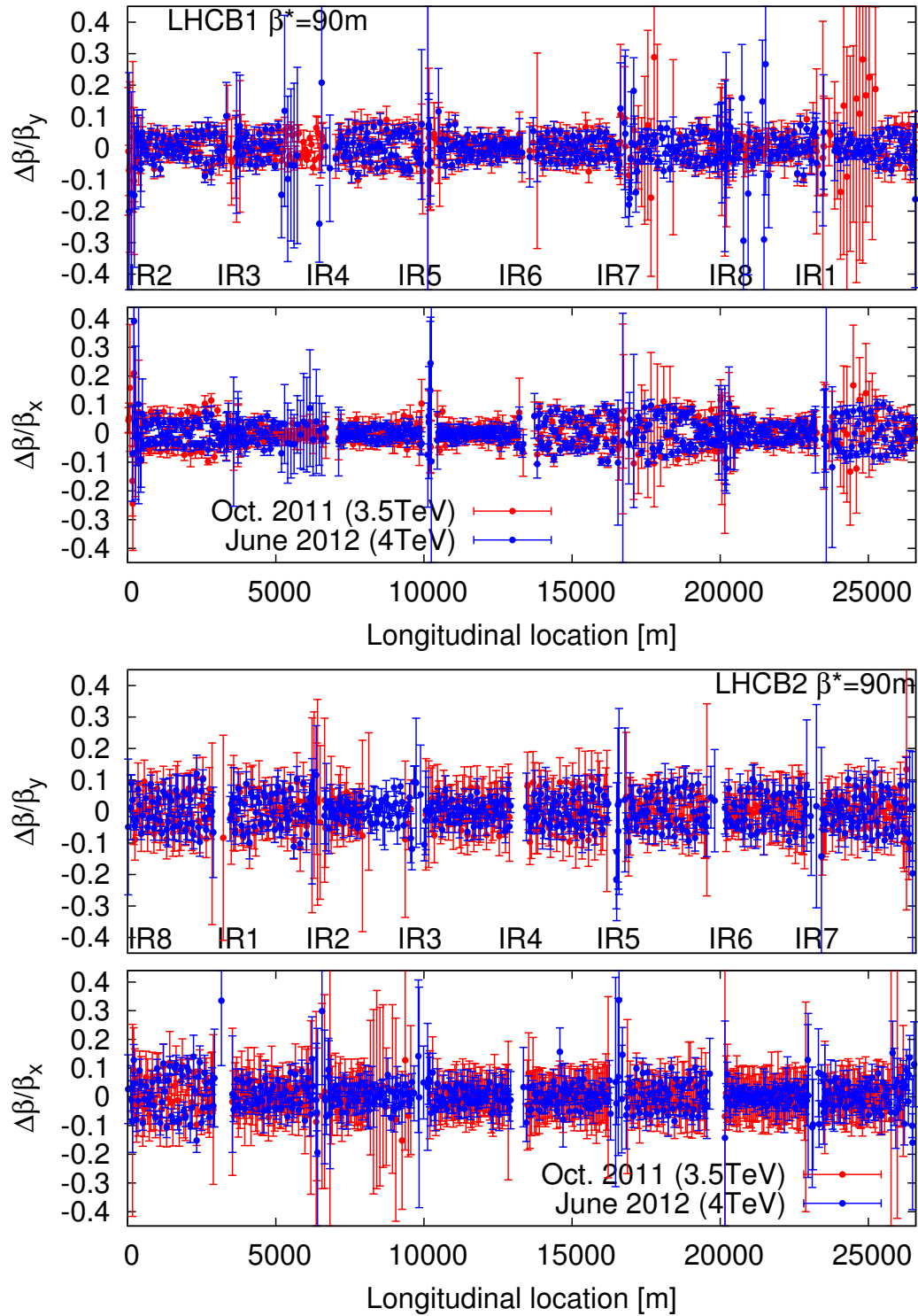


Figure 3.2: A comparison of the  $\beta$ -beat between 2011 and 2012 for the  $\beta^* = 90\text{m}$ . The upper plot shows Beam 1 and the lower plot shows Beam 2.

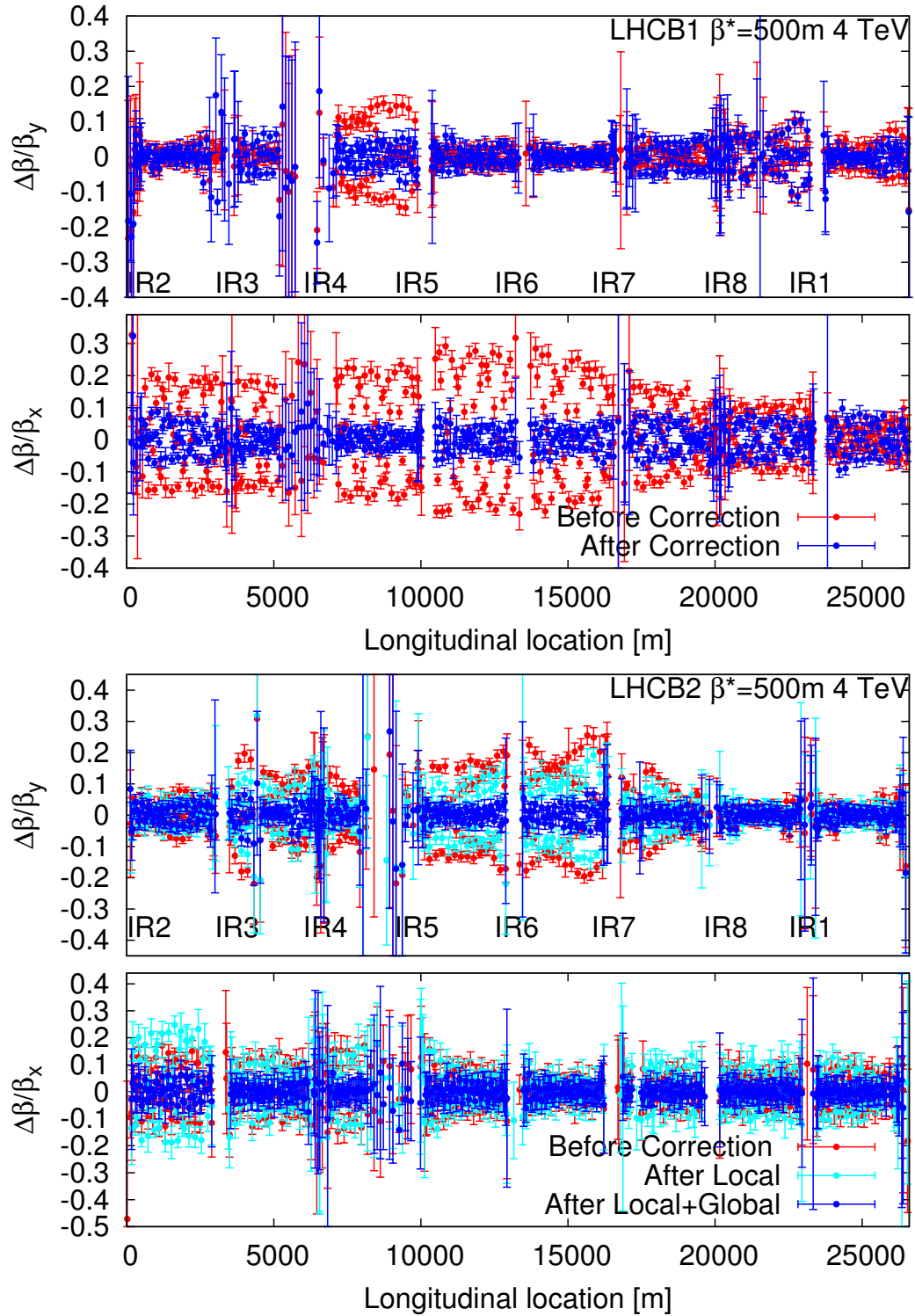


Figure 3.3: A comparison of the  $\beta$ -beat before and after correction for the two beams.

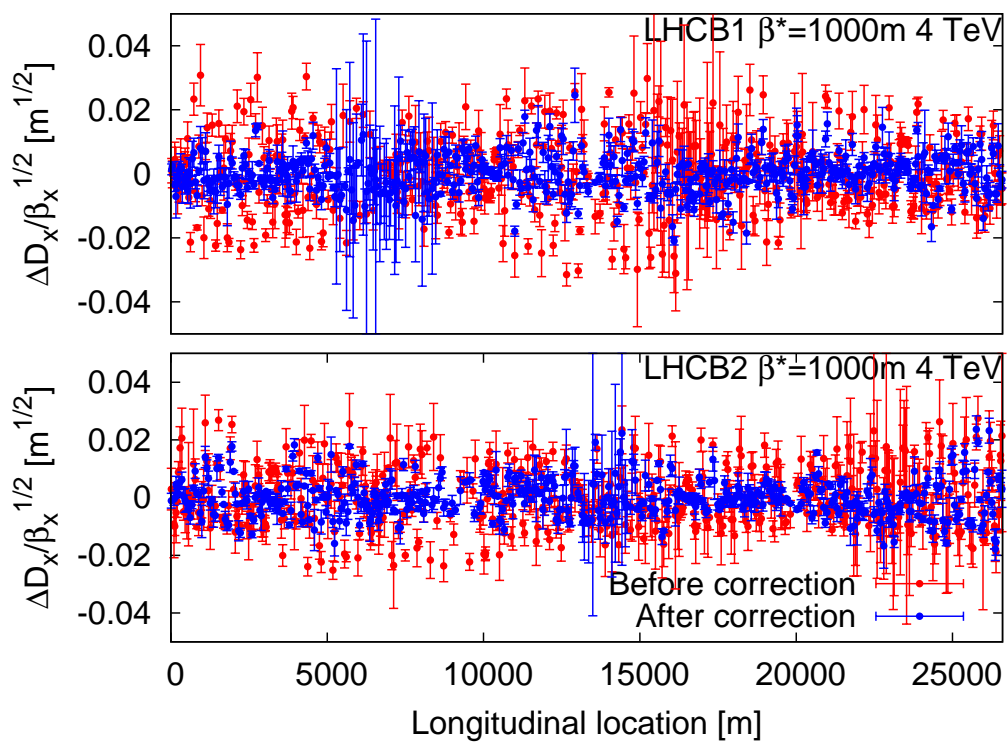


Figure 3.4: The horizontal normalized dispersion before and after correction. The top plot shows Beam 1 and the bottom plot shows Beam 2.

# Chapter 4

## Linear Coupling Corrections

In the absence of transverse coupling motion in the horizontal and the vertical planes are independent. Any field where the position in one plane has an impact on the motion of the other plane will introduce transverse coupling. Unwanted skew quadrupolar fields, which is the dominant source of coupling in the LHC, derive from normal quadrupoles mounted with a rotation, imperfection in the field quality from other magnets and feed down from higher order magnets. It is important to control the coupling since it disturbs the tune feedback and can push tunes into resonances or simply lead to a reduction in the dynamic aperture [48]. In order to correct the coupling skew quadrupoles have been installed throughout the LHC.

In this chapter methods to correct coupling in circular machines are presented. It starts with the dynamics of coupled beam motion followed by a description of how the strength of the skew quadrupoles relates to the  $C^\pm$ . The chapter continues with an explanation of how to measure the  $f_{1001}$  and  $f_{1010}$  from TbT data with special focus on newly developed improvements in the reconstruction algorithm. Finally, the procedure to correct the coupling in the LHC will be presented with special attention to the recently implemented automatic coupling corrections based on injection oscillations. The design of a new coupling feedback designed to be used in the LHC beyond 2015 will also be presented.

### 4.1 Coupled Motion

Linear coupling drives two resonances  $(Q_x - Q_y) = p$  and  $(Q_x + Q_y) = p$ . In the vicinity of the sum and the difference resonances the beam dynamics is strongly influenced. In [49, 17] this is investigated through Hamiltonian perturbation theory and in [50] through resonance driving terms formalism. When the tune split approaches the difference resonance the emittance is described by [17]

$$(\epsilon_x + \epsilon_y) = \text{const} \quad . \quad (4.1)$$

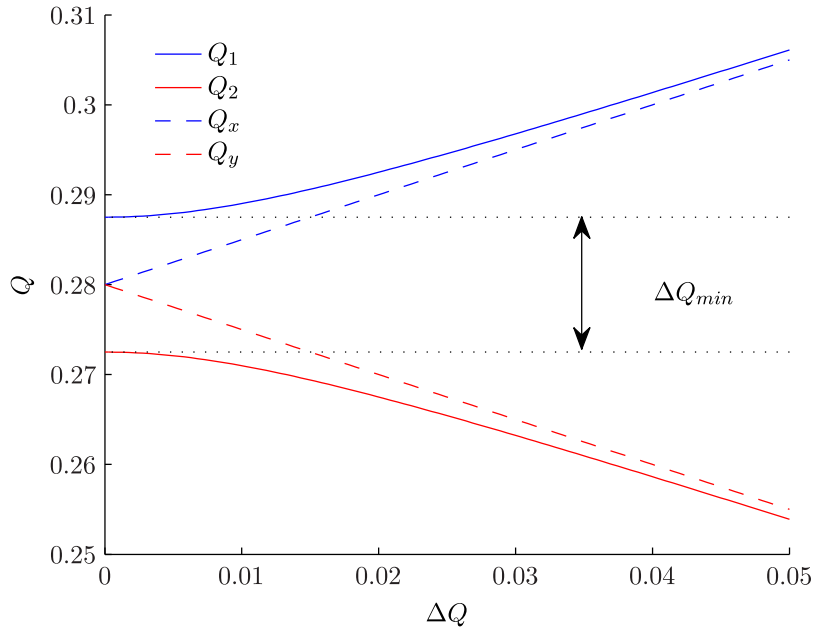


Figure 4.1: The perturbed and unperturbed tunes in the vicinity of the difference resonance in presence of a  $\Delta Q_{min} = 0.015$ .

From this we observe that the beam motion remains stable since neither of the two planes' emittance are allowed to grow unbounded. Instead a periodic exchange of emittance occur between the two planes which gives rise to a beating of the amplitude. This beating may be used to characterize the strength of the coupling and has been used in KEK [51]. In situations where the beam decoheres rapidly this method is not applicable.

The relation between the unperturbed tunes  $Q_{x,y}$  and the perturbed tunes  $Q_{1,2}$  is described by the following equation [52]:

$$\begin{aligned} Q_1 &= Q_x - \frac{\Delta}{2} + \frac{\sqrt{\Delta^2 + |C^-|}}{2} \\ Q_2 &= Q_y + \frac{\Delta}{2} - \frac{\sqrt{\Delta^2 + |C^-|}}{2} \end{aligned} \quad , \quad (4.2)$$

where  $\Delta$  is the unperturbed fractional tune split and  $|C^-|$  is a parameter describing the global coupling and is by definition equal to  $\Delta Q_{min}$ . If  $\Delta \gg |C^-|$  the observed oscillations modes  $Q_{1,2}$  are almost identical to the uncoupled horizontal and vertical tunes  $Q_{x,y}$ . When the tunes are moved closer together the perturbed tunes are forced apart by the coupling. The effect on the perturbed and unperturbed tunes in the vicinity of the difference resonance is shown in figure 4.1.

It is possible to correct the coupling by minimizing the  $\Delta Q_{min}$ . This can be done through pushing the tunes as close as possible together while varying the strength of the skew quadrupoles [51].

## 4.2. From $k_s$ to $C^\pm$

---

When the sum of the fractional tunes approaches an integer the emittance exchange is described by Eq. (4.3) [17].

$$(\epsilon_x - \epsilon_y) = \text{const} \quad (4.3)$$

The sum resonance allows for unstable motion as it is only the difference of the emittance of the two planes that is bounded. The emittance in one plane can increase as long as the other plane increases with equal amount. As a consequence it is commonly chosen to have a working point in an accelerator far from the sum resonance.

## 4.2 From $k_s$ to $C^\pm$

In this section the relation between the skew quadrupolar and the coupling parameters  $C^-$  and  $C^+$  is described. A discussion on the tunes' influence on the relative strength of  $C^-$  and  $C^+$  will also be presented.

In the vicinity of the resonances the  $C^+$  can be calculated from the following equation [48, 25]

$$C^+ = -\frac{1}{2\pi} \oint ds k(s) \sqrt{\beta_x \beta_y} e^{-i(\phi_x + \phi_y) + is(Q_x + Q_y - p_\pm)/R} \quad , \quad (4.4)$$

and the  $C^-$  as

$$C^- = -\frac{1}{2\pi} \oint ds k(s) \sqrt{\beta_x \beta_y} e^{-i(\phi_x - \phi_y) + is(Q_x - Q_y - p_\pm)/R} \quad , \quad (4.5)$$

where  $k(s)$  is the normalized gradient of the skew quadrupole (in units of  $m^{-2}$ ),  $\beta_{x,y}$  are the uncoupled beta functions,  $\phi_{x,y}$  are the horizontal and vertical betatron phases,  $Q_{x,y}$  are the horizontal and vertical betatron tunes,  $p_\pm$  is an integer such that  $(Q_x \pm Q_y)$  is fractional and  $R$  is such that  $2\pi R = \oint ds$ .

It was suggested in [53] that the integer tune split is of greater importance than the fractional tune split to determine the relative strength between the  $C^-$  and the  $C^+$ . The following part contains an investigation of the relative strength in a simplified case. The term  $k(s)\sqrt{\beta_x\beta_y}$  appears both in Eq. (4.4) and Eq. (4.5). Assume a situation where  $k(s)\sqrt{\beta_x\beta_y} = \alpha$ , where  $\alpha$  is a positive constant independent on  $s$ , resulting in a smooth distribution of the coupling. The equation is then described as

$$C^\pm = -\frac{1}{2\pi} \oint ds \alpha e^{-i(\phi_x \pm \phi_y) + is(Q_x \pm Q_y - p_\pm)/R} \quad . \quad (4.6)$$

In order to simplify the equation further assume that the phase is increasing linearly along the machine. Mathematically this is described by the following parametrization:  $\phi_x(s) = Q_x s/R$  and  $\phi_y(s) = Q_y s/R$ , which gives the following integral

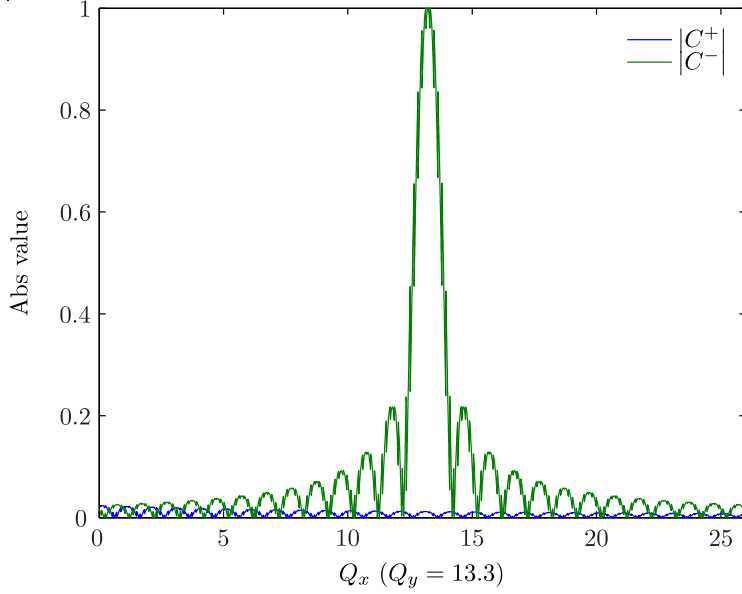


Figure 4.2: A comparison of the relative strength of the  $|C^+|$  and  $|C^-|$  as a function of the  $Q_x$  when  $Q_y = 13.3$ .

$$C^\pm = -\frac{1}{2\pi} \oint ds \alpha e^{-i(Q_x \pm Q_y - (Q_x \pm Q_y - p_\pm))s/R} \quad (4.7)$$

Evaluating the integral yields

$$C^\pm = \frac{R\alpha}{i2\pi} \frac{e^{-i(Q_x \pm Q_y - (Q_x \pm Q_y - p_\pm))s/R} \Big|_0^R}{Q_x \pm Q_y - (Q_x \pm Q_y - p_\pm)} \quad (4.8)$$

Inserting the limits and taking the absolute value of the equation yields

$$|C^\pm| = \frac{R\alpha}{2\pi} \left| \frac{e^{-i(Q_x \pm Q_y - (Q_x \pm Q_y - p_\pm))} - 1}{Q_x \pm Q_y - (Q_x \pm Q_y - p_\pm)} \right| \quad (4.9)$$

Figure 4.2 shows  $|C^\pm|$  calculated from Eq. (4.9) with a vertical tune fixed at 13.3,  $\alpha = 1 \text{ m}^{-1}$  and  $R = 1 \text{ m}$ . It is observable that for small integer tune splits the  $|C^-| \gg |C^+|$ , in general and in cases where  $Q_x + Q_y \approx Q_x - Q_y$  the  $|C^-| \approx |C^+|$ . It is also observable that the fractional tune plays a role in the strength of the  $|C^\pm|$ .

In a realistic case it is necessary to take into account the distribution of the skew quadrupolar fields and the  $\beta$ -functions at those locations to be able to evaluate the strength of the two resonances.

### 4.3 Measuring the $f_{1001}$ and $f_{1010}$

In chapter 2 an introduction was given to the RDTs and how they are inferred from the FFT spectrum of the complex variable. The complex Courant-Snyder

variable is defined as [54]

$$h_{x,-} = \hat{x} - i\hat{p}_x \quad , \quad (4.10)$$

where  $\hat{x}$  is the normalized horizontal position and  $\hat{p}_x$  is the horizontal transverse momentum. The momentum is not a directly measurable quantity with a BPM but needs to be reconstructed using two BPMs. The momentum at the  $i$ th BPM can be written as [50]

$$\hat{p}_{xi} = \frac{\hat{x}_{i+1} - \hat{x}_i \cos \Delta\phi_x}{\sin \Delta\phi_x} \quad , \quad (4.11)$$

where  $\Delta\phi_x$  is the horizontal phase advance between the  $i$ th and  $(i+1)$ th BPM under the assumption that the region between the two BPMs is free of coupling sources and nonlinearities contributing to the main line and the coupling line. Traditionally the momentum has been reconstructed using two consecutive BPMs. In Paper III the benefits with selecting BPM pairs with a phase advance close to  $\frac{\pi}{2}$  for coupling measurements is presented.

It is also possible to approximate the RDTs from the real coordinates but on the expense that some of the lines are inseparable. For the linear coupling it means that the  $f_{1001}$  and  $f_{1010}$  will contribute to the same resonance line. Figure 4.3 shows the vertical FFT spectrum for a kicked beam. In the real spectra (only 1 BPM), shown in figure 4.3(a) it is observed that the spectral lines are mirrored at the 0.5 line. This is not the case for the complex spectra, shown in figure 4.3(b), where 2 BPMs are used to reconstruct the transverse momentum. From the spectral lines shown in figure 4.3 it is possible to calculate the amplitude of the RDTs. The amplitudes can be calculated as [55]

$$|f_{1001}| = \frac{1}{2} \sqrt{\frac{H(0,1)V(1,0)}{V(0,1)H(1,0)}} \quad (4.12)$$

$$|f_{1010}| = \frac{1}{2} \sqrt{\frac{H(0,-1)V(0,-1)}{V(0,1),H(1,0)}} \quad (4.13)$$

and the phase as

$$\begin{aligned} q_{1001} &= \phi_{V(1,0)} - \phi_{H(1,0)} + \frac{\pi}{2} = \phi_{H(0,1)} - \phi_{V(0,1)} + \frac{\pi}{2} \\ q_{1010} &= \phi_{H(0,-1)} - \phi_{V(0,1)} + \frac{\pi}{2} = \phi_{V(-1,0)} - \phi_{H(1,0)} + \frac{\pi}{2} \quad . \end{aligned} \quad (4.14)$$

From the phase and the amplitude information the complex RDTs are constructed as  $f_{1001} = |f_{1001}|e^{iq_{1001}}$  and  $|f_{1010}| = e^{iq_{1010}}$ . When only the real variable is used it is not possible to separate the  $f_{1001}$  from the  $f_{1010}$  but depending on the relative strength between the two it might be possible to neglect one of them. In figure 4.3 it is observed that the amplitude of the  $V(1,0)$  is similar for the real and the complex spectra and that  $f_{1010}$  is considerably smaller. This shows that in this case the  $|f_{1001}| \gg |f_{1010}|$ .

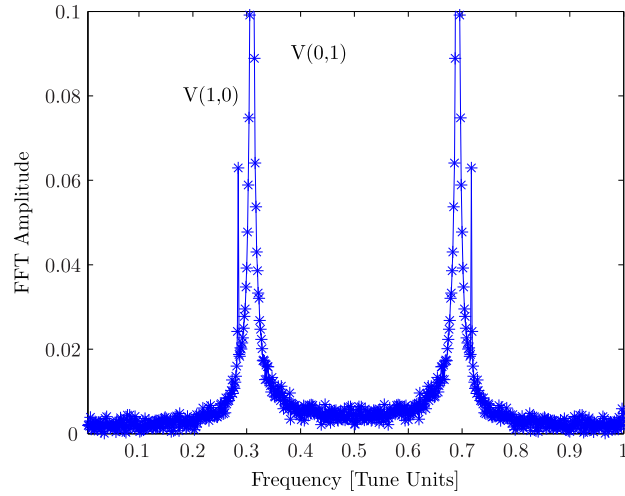
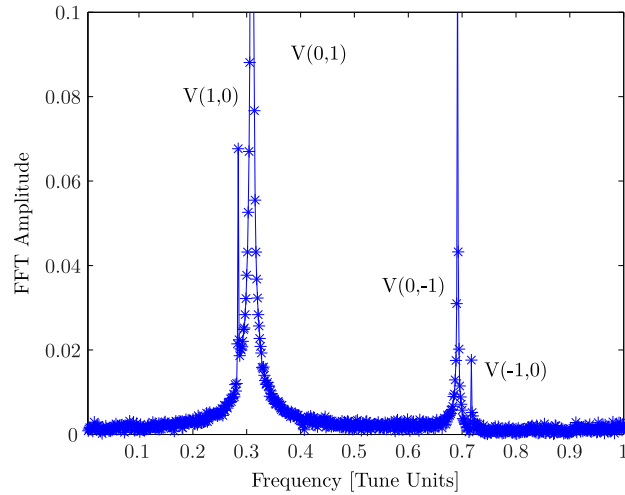

 (a) Real spectra normalized to  $V(0,1)$ .

 (b) Complex spectra normalized to  $V(0,1)$ .

Figure 4.3: The vertical FFT spectra from injection data from the real variable (1 BPM) and the complex spectra (reconstructed from 2 BPMs).

In the following part a comparison of the coupling RDT reconstructed from a real variable and from the complex Courant-Snyder variable is given. Figure 4.4(a) shows a simulation performed in Polymorphic Tracking Code (PTC) comparing the calculation of  $f_{1001}$  based on 1 BPM and 2 BPMs. It is evident that the 2 BPMs method is better in reconstructing the  $f_{1001}$ . The mixing with the  $f_{1010}$  is, however, relatively small due to the small fractional tune split. The amplitude of a RDT is increasing as the tunes are approaching the resonance condition. In figure 4.4(b) the same simulation is performed but in this case the fractional tunes are changed away from the difference resonance and closer to the sum resonance. From this simulation it is clear that at such an operation

### 4.3. Measuring the $f_{1001}$ and $f_{1010}$

point approximating the  $f_{1001}$  from 1 BPM would cause significant errors.

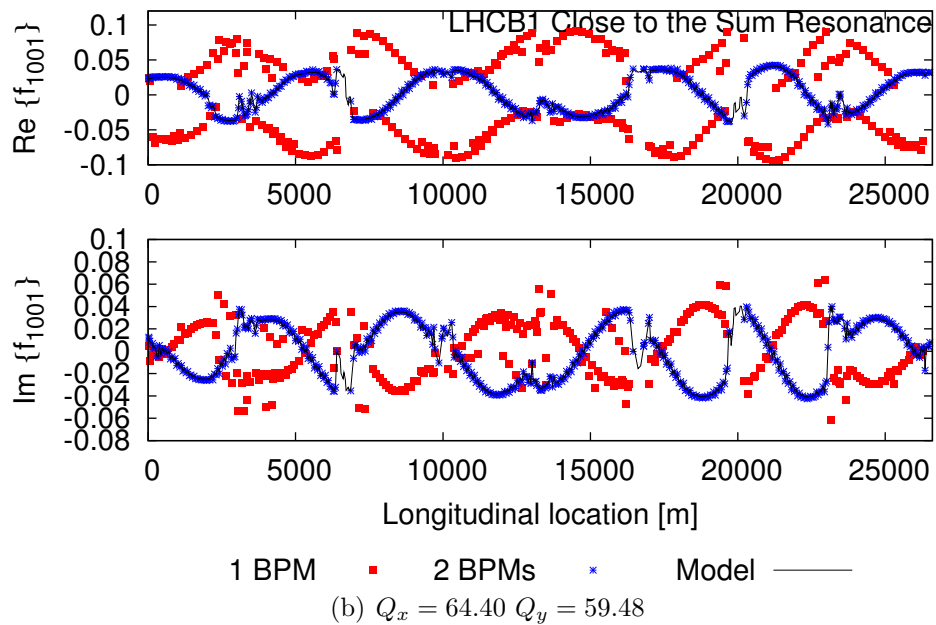
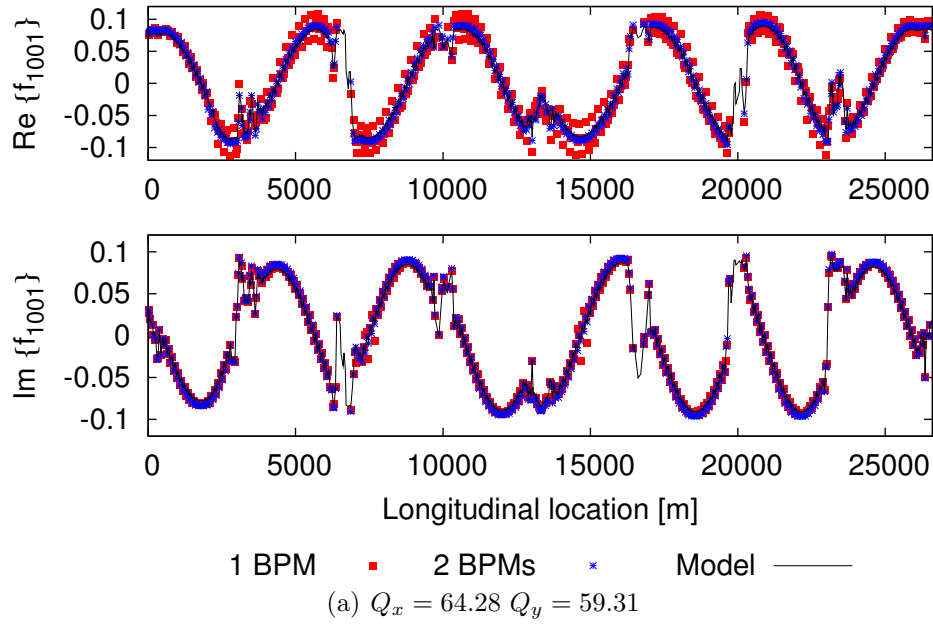


Figure 4.4: A comparison of the 1 BPM and 2 BPMs methods to reconstruct the  $f_{1001}$ .

## 4.4 Correction Procedure in the LHC

The correction procedure in the LHC is to first correct the strong local coupling sources and then correct the global coupling. The local correction has remained constant during the 2012 run while the global coupling was corrected on a weekly basis.

All coupling measurements presented in this thesis are based on TbT data which is first cleaned using a Singular Value Decomposition (SVD) algorithm. In Paper III an investigation on how to optimally clean the data using SVD is presented. The spectrum is then obtained from SUSSIX [56] and the RDTs are calculated [55].

### 4.4.1 Local Coupling Correction

A local correction aims at correcting the coupling in the region where it occurs. The local correction relies on the fact that the amplitude of the RDTs stays constant in regions without coupling sources and shows abrupt jumps at the locations of these sources [24]. The analytical expression describing these abrupt changes are given in [57] and [58] as

$$f_{jklm}^{(2)} = e^{-i[(k-j)\Delta\phi_x + (m-l)\Delta\phi_y]} \left[ f_{jklm}^{(1)} - \sum_{q=1}^n e^{i(k-j)\phi_{xq} + i(m-l)\phi_{yq}} h_{q,jklm} \right], \quad (4.15)$$

where  $f_{jklm}^{(2)}$  are the RDTs at a second location,  $\Delta\phi_{x,y}$  are the horizontal and vertical phase advances between the two locations, the summation extends only over the multipoles placed in between the two locations,  $\phi_{xq,yq}$  are the phase advances between the first location and the  $q^{\text{th}}$  multipole and  $h_{q,jklm}$  are real quantities proportional to the integrated strength of the  $q^{\text{th}}$  multipole and to the product  $\beta_{xq}^{\frac{j+k}{2}} \beta_{yq}^{\frac{l+m}{2}}$ .

The local coupling corrections are calculated in regions where abrupt changes are observed, normally close to the IPs. The method was first presented in [59]. The coupling RDTs are plotted and compared to the model using the first RDTs as the starting conditions. The amplitude of the coupling RDTs are constant in our ideal model but by introducing errors in the model the measured situation is reproduced. The correction is then applied to the machine with opposite sign. An example of a local correction of IP2 from the commissioning in 2012 is shown in figure 4.5. When a local correction is calculated in the IP region it also has to be validated that the same correction is valid for both beams.

Figure 4.6 shows the coupling situation before and after the local corrections were applied. The overall amplitude of the coupling has decreased but even more significant is that the abrupt changes have decreased. This is very important in order to use a global correction approach to correct the coupling.

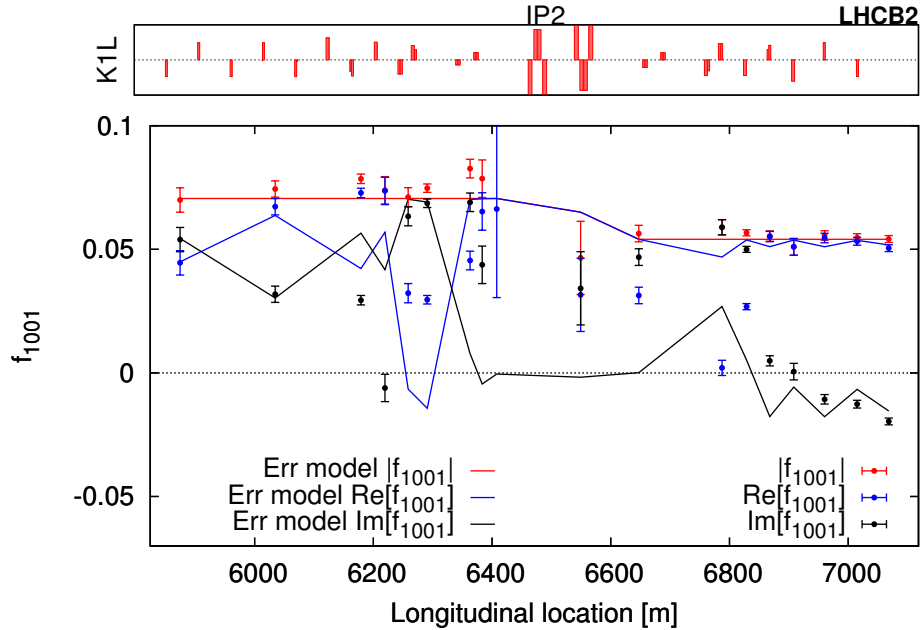


Figure 4.5: The measured coupling RDTs close to IP2 together with the introduced error in the model to reproduce the measurement.

#### 4.4.2 Global Corrections

The global coupling has been corrected via two knobs which control the real and imaginary part of the  $C^-$  respectively [60].

Figure 4.7 shows a simulated comparison of the coupling situation in case a global correction is applied with and without a local correction. It is observed that the global corrections are able to correct the situation better after the local corrections are applied. This is due to the fact that the global coupling corrections assume that the coupling is distributed along the machine.

In practice the settings of the knobs were changed by the operator in an iterative manner while observing the  $|C^-|$  measured from a single dedicated high precision pickup, BBQ [61]. This approach is suffering from two drawbacks. First, it is only possible to measure the amplitude of the coupling, which means that the operator has to scan the knobs to find the optimal setting. Second, it fully relies on the measurement at a single location by a single BPM. This can be deceiving since correcting the coupling locally does not guarantee that it is minimized globally, plus a single BPM does not allow to distinguish between the  $f_{1001}$  and the  $f_{1010}$ .

##### 4.4.2.1 Automatic Coupling Corrections Based on Injection Oscillations

Instead of manually adjusting the coupling knobs a method was developed to measure the coupling based on the injection oscillations and then automatically

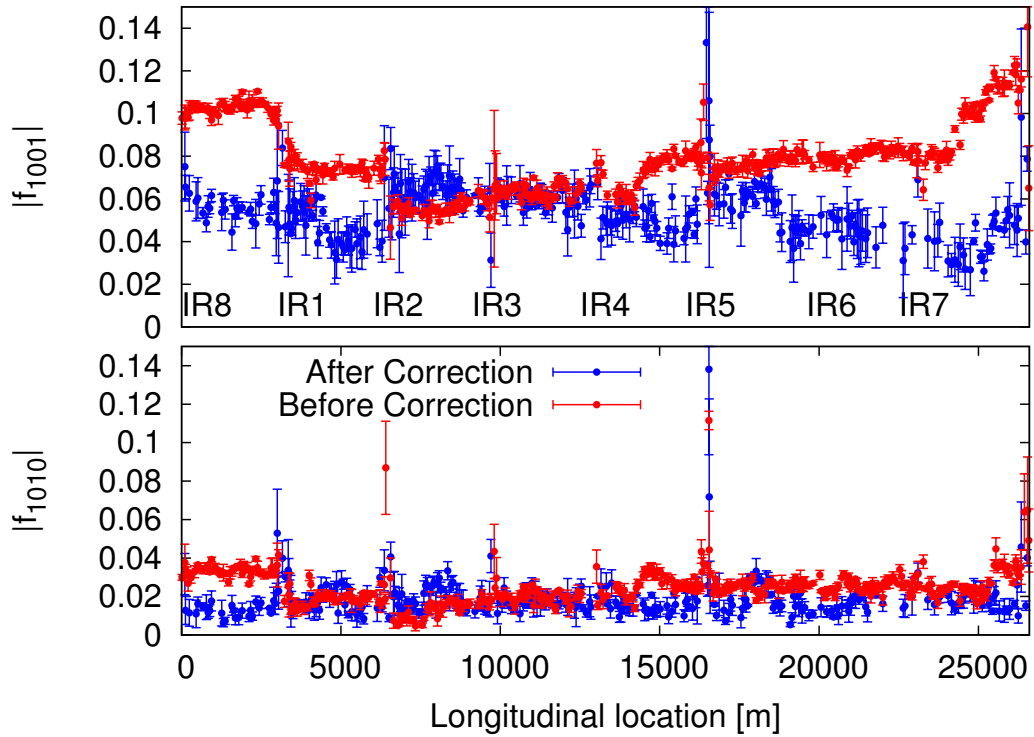


Figure 4.6: The  $f_{1001}$  before and after the local correction.

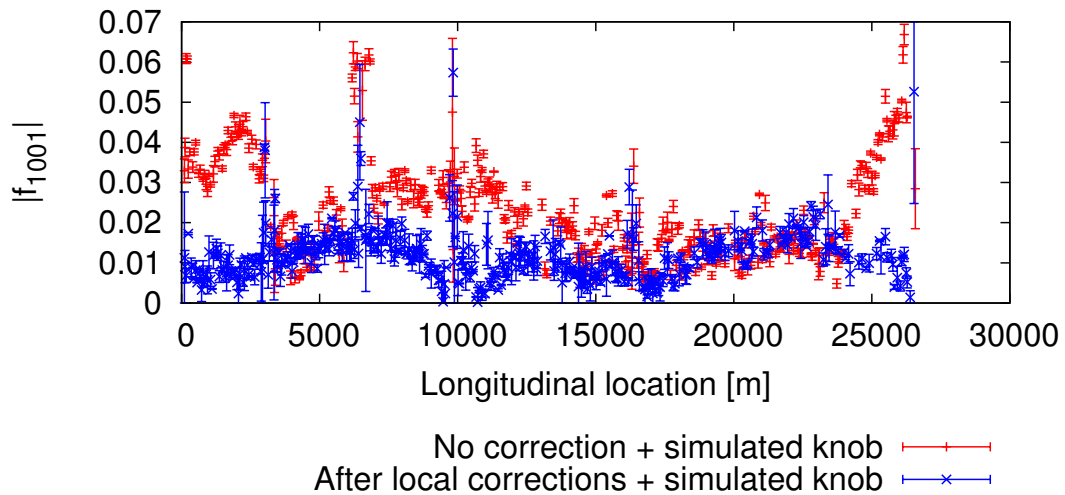


Figure 4.7:  $f_{1001}$  before and after local corrections after applying a simulated correction with the global knobs.

calculate a correction. The software was designed in such a way that the necessary calculations were performed as soon as the TbT data was available. A user interface was then designed to display the suggested corrections to the operator. In this way it was avoided that the operator would have to wait 30 s every time they would like to correct the coupling. The automatic coupling corrections based on the injection oscillations are used in normal operation of the LHC and described in detail in Paper III and in Paper IV.

### 4.4.2.2 Coupling Feedback

The injection oscillations provide measurements for correction of the global coupling. It can, however, only provide measurements at injection. In order to have a measurement also at any other time in the LHC cycle different possibilities were investigated [62, 63]. The outcome of the study was to use newly developed electronics for precise position measurements. The system is called Diode Orbit and Oscillation (DOROS) and 10 BPMs for each beam are foreseen to be equipped with this electronics. The locations of the BPMs are, however, not optimized for coupling measurements since the phase advance is far from the optimal  $\frac{\pi}{2}$ . Instead a different layout, based on the information from all the BPMs but only using the real spectrum, was chosen. The layout of this foreseen coupling feedback is presented in Paper III.

### 4.4.3 The Influence of Coupling on $\beta$ -beat

It is clear from section 2.5 that a skew quadrupole also has an influence on the  $\beta$ -functions. In figure 4.8 the  $\beta$ -beat caused by introducing an coupling situation in the model is shown. The induced  $\beta$ -beat is below 0.15% for a  $|C^-| = 0.01$ . As a consequence it is possible to correct and adjust the coupling without affecting the  $\beta$ -beat to any significant level.

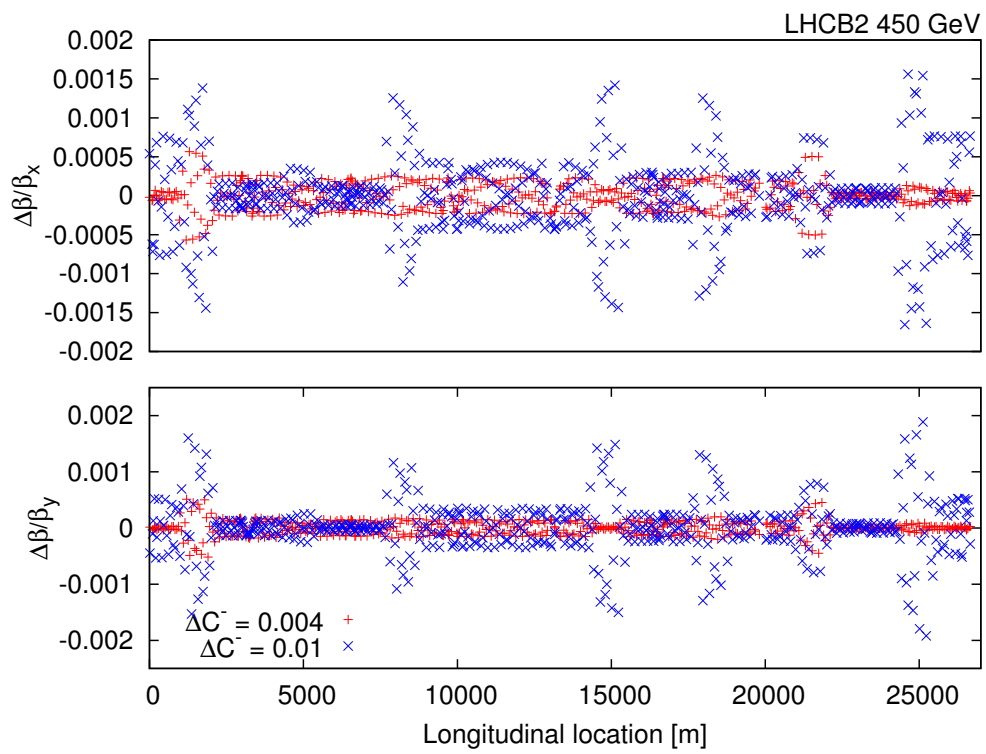


Figure 4.8: The influence of the  $C^-$  on the  $\beta$ -beat

# Chapter 5

## Chromatic coupling

Energy dependent coupling, termed chromatic coupling, is generated by sextupolar fields in magnets, in combination with dispersion. An off-momentum particle will experience a skew quadrupolar field from a sextupole in dispersive regions (vertical dispersion and normal sextupole, or horizontal dispersion and skew sextupole). An example of an ideal sextupole and a skew sextupole is given in figure 5.1.

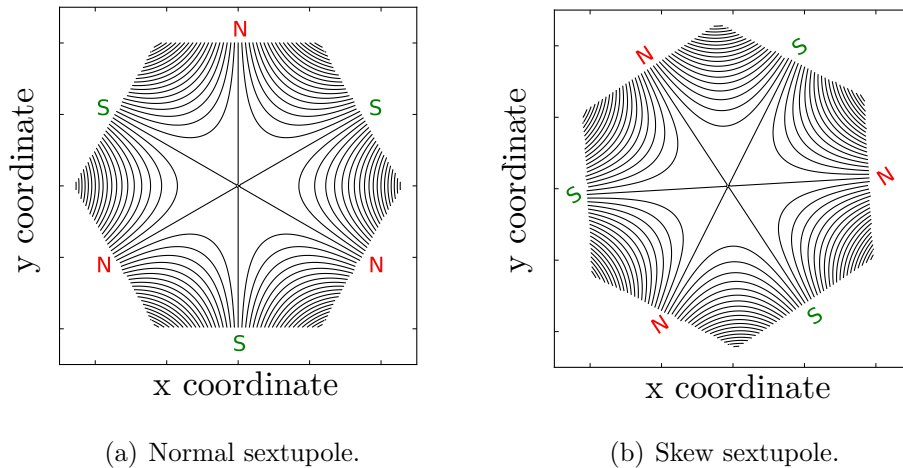


Figure 5.1: The magnetic field lines for ideal normal and a skew sextupole. Note that the rotation of the skew sextupole is  $\frac{\pi}{6}$  compared to the normal.

It was shown early on in theoretical studies of the LHC that chromatic coupling would be a significant source of perturbation at injection [64, 65, 66], due to a large skew sextupolar component in the arc dipoles. Consequently, skew sextupoles were installed in all arcs to provide the possibility to correct the chromatic coupling.

## 5.1 From Sextupolar Fields to Chromatic Coupling

A beam passing off-center through a magnet will, in addition to the expected fields for that multipole, experience fields of all lower orders. This effect is termed feed-down and causes, for example, a particle passing off-center in a quadrupole to receive a dipole-kick. In the following section an explanation of how sextupoles feed-down to a skew quadrupolar component and in combination with dispersion give rise to chromatic coupling.

From Eq. (2.17) the magnetic field from a normal sextupole and a skew sextupole are described as

$$N_3 = \text{Re}[(x + iy)^3] = x^3 - 3y^2x \quad (5.1)$$

$$S_3 = \text{Im}[(x + iy)^3] = -y^3 + 3yx^2 \quad (5.2)$$

We follow the approach described in [17] in order to investigate the effect of passing off-center in a skew sextupole. The transformation  $x \rightarrow x - \Delta x$  is made, where  $\Delta x$  represents the offset in the skew sextupole. Using Eq. (2.16) and performing a Taylor expansion about  $\Delta x = 0$ , modifies the term in the Hamiltonian to:

$$\mathbf{N}_{\mathbf{3},\mathbf{3} \rightarrow \mathbf{2}}(\Delta \mathbf{x}) = \frac{q}{p} \frac{1}{3} B_3 [(-y^3 + 3yx^2) - \Delta x(6xy) + \mathcal{O}(\Delta x^2)] \quad , \quad (5.3)$$

which also can be expressed as

$$\mathbf{N}_{\mathbf{3},\mathbf{3} \rightarrow \mathbf{2}}(\Delta \mathbf{x}) = \mathbf{N}_{\mathbf{3}} + \frac{q}{p} \frac{1}{3} B_3 [\Delta x \text{Im} [(x + iy)^2]] + \mathcal{O}(\Delta x^2) \quad . \quad (5.4)$$

From Eq. (2.17) it is found that  $\mathbf{S}_{\mathbf{2}} \propto \text{Im} [(x + iy)^2]$ , demonstrating that the first order horizontal feed-down from a normal sextupole gives a skew quadrupole term in the Hamiltonian. The higher order terms in the expansion give rise to dipole-like terms. Since the position at a dispersive location by definition is dependent on the energy,  $\Delta x$  will vary for particles with different energies and hence give rise to chromatic coupling. In Eq. (5.2) we observe that the the difference between the normal and skew sextupole is only a sign when changing  $x$  with  $y$ . This makes us conclude that performing the same calculation for a normal sextupole with vertical dispersion will again give rise to a skew quadrupolar component in the Hamiltonian. Since there is larger horizontal dispersion in the LHC, and in rings generally, skew sextupolar components are the dominant source of chromatic coupling. Also note that higher order fields may feed-down to sextupolar fields and hence give rise to chromatic coupling.

## 5.2 Motivation

Improving chromatic coupling will generally improve lifetime and control of the beam. Chromatic coupling creates a dependency between the tune and the momentum, which deteriorates the beam quality and reduces the available dynamic aperture [65, 67]. The chromatic coupling also has a direct influence on the  $|C^\pm|$  since a beam has an energy spread and as a consequence the different particles experience different coupling. This effect is not directly measurable in normal operation, without changing the energy, but does contribute to the dynamics of the off-momentum particles.

An increase in luminosity of 20% after local chromatic coupling correction of the IP in KEKB was reported in [68, 69]. The effect of a correction is not expected to be as pronounced for the LHC since transverse round beams are collided instead of flat beams.

## 5.3 Measurement and Correction Procedure

Measurements and corrections of chromatic coupling were performed for the first time in the LHC in 2012. The method used was to measure the  $f_{1001}$  for different energies and then calculate corrections based on our model. The method and the corrections are presented in Paper V. The paper also compares the results to expectations from the magnetic model of the LHC.



# Chapter 6

## CLIC

In this chapter an investigation of how the requirements for a multi-TeV  $e^+e^-$  collider have driven the design of CLIC will be presented. A description of the layout and the key components will also be given.

### 6.1 Requirements that Drive the Design

The optimization of the CLIC design has been done with the focus on a  $\sqrt{s} = 3\text{ TeV}$  machine. It is more likely, however, that the starting energy would be  $\sqrt{s} = 350\text{ GeV}$  and then extended first to reach  $\sqrt{s} = 1.5\text{ TeV}$  and then finally to  $\sqrt{s} = 3\text{ TeV}$ .

The particle physics community has requested an even higher luminosity for the future linear collider than achieved in the LHC. The design luminosity is  $\mathcal{L} = 5.9 \times 10^{34}\text{ cm}^{-2}\text{s}^{-1}$  for the 3 TeV option [19]. In order for the project to be feasible it is important to minimize both construction costs and running costs.

#### 6.1.1 Reaching the TeV-scale

In a linear machine each cavity will only accelerate the particles once. The two ways to increase the energy are to build the machine longer or to increase the accelerating field strength. An increase in length is associated with extra cost, for tunnelling and extra material. This makes it preferable to increase the field strength. The limit on achievable fields for superconducting cavities imply a  $\sim 150\text{ km}$  long accelerator to achieve  $\sqrt{s} = 3\text{ TeV}$  [70]. With normal conducting accelerating cavities it is possible to reach higher gradients. The accelerating gradient for CLIC was chosen to be  $100\text{ MV/m}$ . This gradient was chosen after a careful optimization of the physics parameters, while minimizing the cost, and keeping the break down rate below  $10^{-7}/\text{m}$  [71]. A higher rate of breakdowns would be problematic as too many beam trains would be lost, hence decreasing the integrated luminosity. The break down rate is very dependent on the RF pulse length. As a consequence the pulse length is limited to  $150\text{ ns}$ .

For the generation of high RF power, only klystrons are, to date, available as power source. There are, however, no klystrons available that can produce the short RF pulses required. The klystrons present on the market deliver roughly an order of magnitude longer RF pulses. The system would need to be combined with networks of RF pulse compressors. Even with this solution the linac would need to be equipped with 35 000 high power klystrons to reach  $\sqrt{s} = 3\text{TeV}$  [19]. This is not feasible in terms of cost, maintainability and power consumption. The scheme foreseen for CLIC will instead rely on the use of a very long but relatively low energy drive beam. The long beam is then folded, through an advanced compression scheme, into a shorter but higher current beam. This beam is then decelerated in special structures and the high fields are transported to the accelerating structures on the Main Beam side. The idea is analogous to a transformer where the high current but low voltage (Drive Beam) is converted into a high voltage but low intensity (Main Beam). With this scheme only 1638 klystrons would be needed [19]. The price to pay is the extra infrastructure and complexity associated with the Drive Beam.

### 6.1.2 Reaching High Luminosity

In a linear collider there is only one chance for the particles to collide. This can be compared to the situation in a circular machine where the bunches cross billions of times. A comparison between the LHC and the CLIC parameters will be given to bring insight to the challenge of creating high luminosity in a linear collider.

The revolution frequency in the LHC is  $\sim 11\text{kHz}$  and there are about  $10^{11}$  particles per bunch. The LHC is designed to have up to 2808 bunches per beam resulting in an average bunch crossing at around 30 MHz. The proposed repetition rate for CLIC is 50 Hz, with 312 bunches per pulse, resulting in an average bunch crossing of 15 kHz. The repetition rate is limited to that ballpark because of costs associated with an increase in power consumption and extra cost for technical systems like the modulators. Table 6.1 compares the LHC and CLIC in terms of parameters that affect their luminosity.

Parameter	LHC	CLIC
average $f_{coll}$	30 MHz	15 KHz
$N_b$	$10^{11}$	$3 \times 10^9$
$f_{coll}N_b^2 \sim$	$3 \times 10^{29}$	$8 \times 10^{22}$

Table 6.1: Table comparing important parameters for luminosity production between the LHC and CLIC,  $f_{coll}$  is the bunch crossing frequency and  $N_b$  is the number of particles per bunch.

If we assume head on collisions of Gaussian-shaped bunches, the luminosity

can be written as [25]

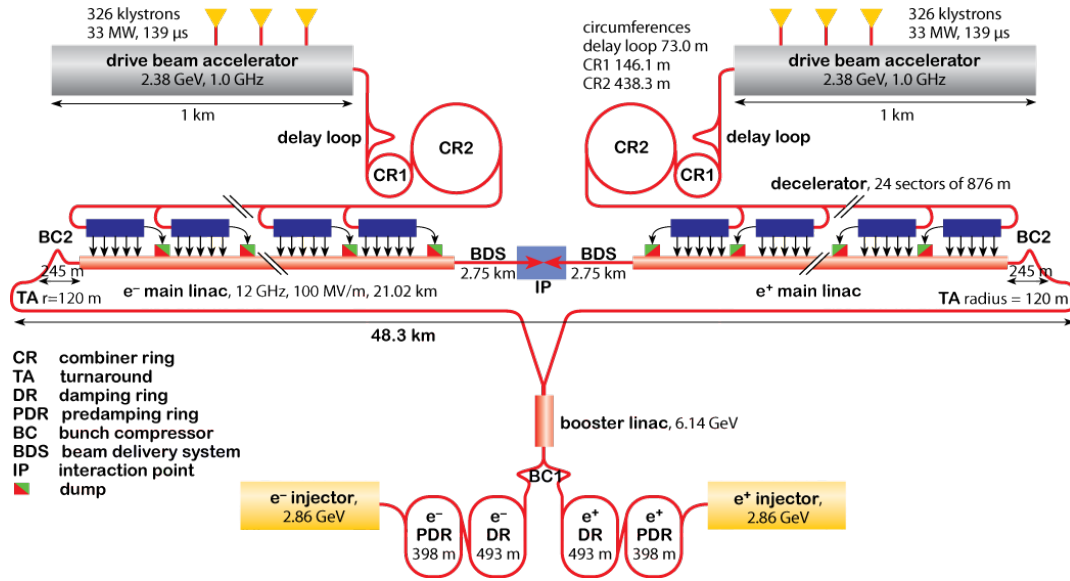
$$\mathcal{L} = \frac{f_{coll} N_b^2}{4\pi\sigma_x\sigma_y} . \quad (6.1)$$

The numerator from Eq. (6.1) is calculated for the LHC and CLIC and presented in table 6.1. By comparing the numbers we see that LHC would produce almost  $10^7$  higher luminosity. The number of particles per bunch is limited by beam dynamics considerations, therefore the only way to increase the luminosity is to shrink the beam size. The beam size is given by  $\sqrt{\beta\epsilon}$ , where  $\epsilon$  is the beam emittance and  $\beta$  is a function of the lattice. The beam size is decreased in two different ways. The first way is through squeezing the beam more at the interaction point, i.e. by reducing the  $\beta^*$ . The second way is by creating beams with smaller emittance compared to the LHC. The total decrease in beam size for CLIC compared to the LHC is in the order of  $10^4$  for the vertical beam size and  $10^3$  for the horizontal. The vertical beam size is then in the order of 1 nm while the horizontal will be 46 nm [19]. In this way it is foreseen to reach even higher luminosity than in the LHC.

In order to deliver high integrated luminosity it is not sufficient to reach the small beam sizes. They also need to be maintained throughout the run. This puts tight constraints on the stability of the beam. One crucial parameter to keep stable is the beam energy of the colliding beams. Since the Main Beam is accelerated with the fields created by the Drive Beam, this in turn puts tight constraints on the Drive Beam. The beam current, the phase and the bunch length all influence the magnitude of the acceleration of the Main Beam. An energy variation of the Main Beam will lead to a decrease in luminosity. This decrease is due to the limited energy bandwidth of Beam Delivery System and due to the increase of the emittance in the main linac. The decrease is observed to be quadratic with respect to the energy variation [72]. The Drive Beam stability's impact on the luminosity makes it an important issue that has to be understood and controlled. In section 7.2, the stability of the CTF3 Drive Beam will be presented together with the improvements made to increase it.

## 6.2 Layout

In figure 6.1 a schematic overview of CLIC is shown. A thermionic gun creates a  $140\ \mu\text{s}$  long and 4.2 A beam. The beam is accelerated with conventional klystrons using special structures operated in fully loaded mode. This gives an RF to beam efficiency of 97% which is crucial for the overall energy consumption [73]. The particles are accelerated to 2.4 GeV before they are sent to the delay loop followed by the combiner rings where the bunch trains are interleaved and combined, giving rise to multiplication in current and frequency. After combination the beam current is 100 A and the frequency 12 GHz. A more detailed description of the combination process is given in section 7.1.1.

Figure 6.1: Overview of the CLIC layout for  $\sqrt{s} = 3$  TeV.

The high current beam is then sent to the different decelerators where it is transferring its energy to the Main Beam.

The electrons for the Main Beam are produced by a thermionic gun while the positrons are created through Compton scattering. Both beams are then accelerated using conventional klystrons before they are sent to the Pre-Damping Ring followed by the Damping Ring. In the damping rings the emittance is reduced, which is crucial to reach the very small beam sizes. Afterwards the beams are accelerated further before they are injected into the main linac. In the main linac they are accelerated with the help of the Drive Beam. They are brought to the Beam Delivery System which focuses the beams to very small beam sizes before they are collided in the detector. The non-colliding particles are then brought to a post-collision line where they are diagnosed before they are dumped.

## Chapter 7

# Experimental Verification at CTF3

The main goal of CTF3 is to experimentally verify the CLIC scheme. In particular, it aims at demonstrating the generation of the high current Drive Beam and its use in the two-beam acceleration [74]. It is also used as a test bench for beam instrumentation and algorithms that could be used for CLIC. Most of the devices in CTF3 are from the old LEP-injector. This allowed for keeping the construction costs down but it also means that the equipment was optimized for a different use.

## 7.1 Layout of CTF3

Figure 7.1 shows the layout of the CTF3 complex. In CTF3 a thermionic gun produces a 4.3 A beam which is bunched in the injector. The bunched beam then passes through a compressor chicane before it is accelerated in the linac. The accelerating frequency in the linac is 3 GHz while the bunch frequency can either be 1.5 GHz or 3 GHz depending on the mode of operation. The acceleration of the beam is done with RF generated by 3 GHz klystrons and amplified by pulse compressors. This gives an increase of peak power by a factor 2 while reducing the pulse length, but also introduces instabilities which will be described in detail in section 7.2. In the linac there are 14 accelerating structures which are operated in fully loaded mode. This mode gives a high RF to beam efficiency but also introduces a correlation between beam current and beam energy. The beam is accelerated to  $\sim 125$  MeV in the 70 m long linac.

The delay-loop and the combiner ring are used to compress the beam in order to increase the frequency and peak current. The recombination scheme is described in section 7.1.1. After the combiner ring the beam is transported towards CLIC Experimental Area (CLEX). In CLEX there are two beam lines, Test Beam Line (TBL) which investigates the effect of deceleration of the Drive Beam. The other line, Two Beam Test Stand (TBTS), is used to test the concept of the two-beam acceleration. It extracts the power from the Drive Beam and uses it to accelerate the CALIFES beam.

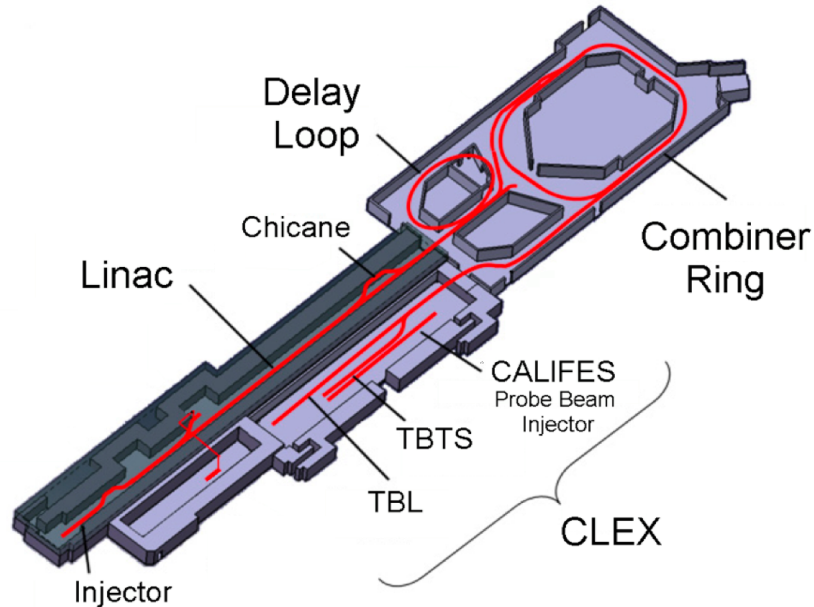


Figure 7.1: Layout of the CTF3 complex.

### 7.1.1 Drive Beam Generation

The CTF3 injector can create a beam with either 1.5 GHz or 3 GHz bunch frequency. In case of the 1.5 GHz beam a phase flip of  $180^\circ$  is introduced every 140 ns by the sub harmonic bunching system. The  $180^\circ$  phase flip in 1.5 GHz translates into a  $360^\circ$  phase flip in 3 GHz. This means that all bunches see the same accelerating gradient in the 3 GHz accelerating structures. At the entrance to the delay loop the beam passes through a 1.5 GHz transverse deflector. The timing between the RF-deflector and beam arrival is synchronized so that the even bunches are injected to the delay loop while the odd bunches bypass, see figure 7.2. In this way the delay loop transforms the long 1.5 GHz bunch train into 4 sub-trains with a bunch frequency of 3 GHz. The delay loop is equipped with wigglers which can be used to ensure the right path-length. This is important in order to obtain the correct bunch distance after the recombination. From the delay loop the beam is transferred to the combiner ring

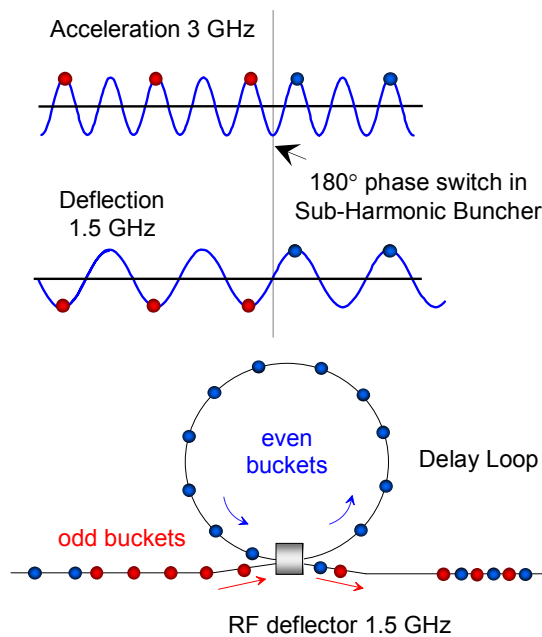


Figure 7.2: The frequency and current multiplication in the delay loop.

where it is combined in a similar manner as for the delay loop. Here, however, the beam is combined 4 times. The total combination factor is then 8 when both delay loop and combiner ring are in use.

In the case the mode of operation is 3 GHz the sub harmonic bunchers are not used. The 3 GHz beam bypasses the delay loop and goes straight to the combiner ring where it is combined 4 times giving a frequency and current multiplication of factor 4. Figure 7.3 shows the recombination process in the combiner ring.

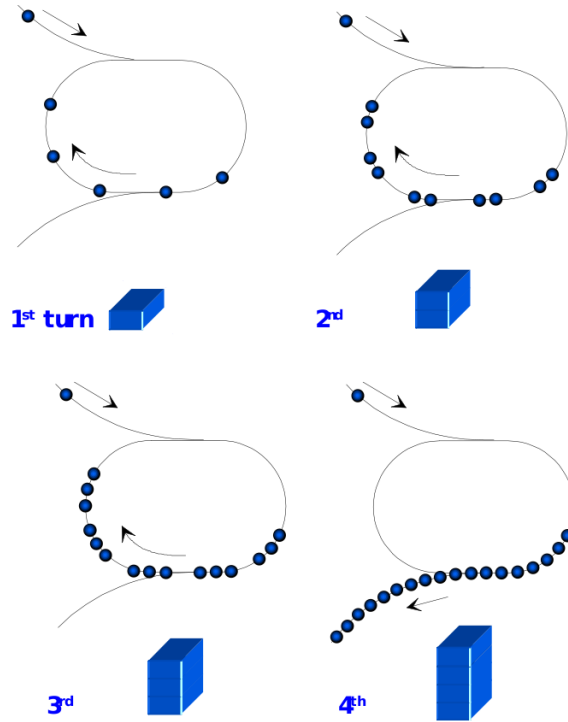


Figure 7.3: A schematic view of the recombination in the combiner ring.

#### 7.1.1.1 Emittance Preservation in the Combiner Ring

One of the targets for CTF3 is to demonstrate a combined beam with emittance below  $150 \pi \mu\text{m}$  for both planes [75]. There are several factors that can increase the emittance in the combiner ring, such as uncontrolled dispersion, unmatched lattice and miss-steering at injection. A study was launched in 2012 to understand where the observed increase was originating from. It was found that injecting onto the closed orbit of the combiner ring was of key importance to minimize the emittance growth. The emittance increase is caused by the large energy spread of the beam in combination with high chromaticity in the combiner ring. The effect of decoherence is shown in figure 2.7 and described in section 2.3. In figure 7.4 the standard deviation around the closed orbit for a short pulse circulating 4 turns is plotted against the horizontal emittance. I varied the magnitude of the oscillations around the closed orbit by changing corrector magnets before the injection. The standard deviation is measured using 5 BPMs, the quoted standard deviation is the mean of these value. It was repeated with a beam combined 4 times. As seen in figure 7.4 the emittance for this beam is larger than for the uncombined beam. The reason is that the different turns have slightly different orbits and hence they are together occupying a larger part of the transverse space. The measurements of the uncombined beam show good agreement with simulations [76].

After a careful setup of the injection and extraction to the combiner ring

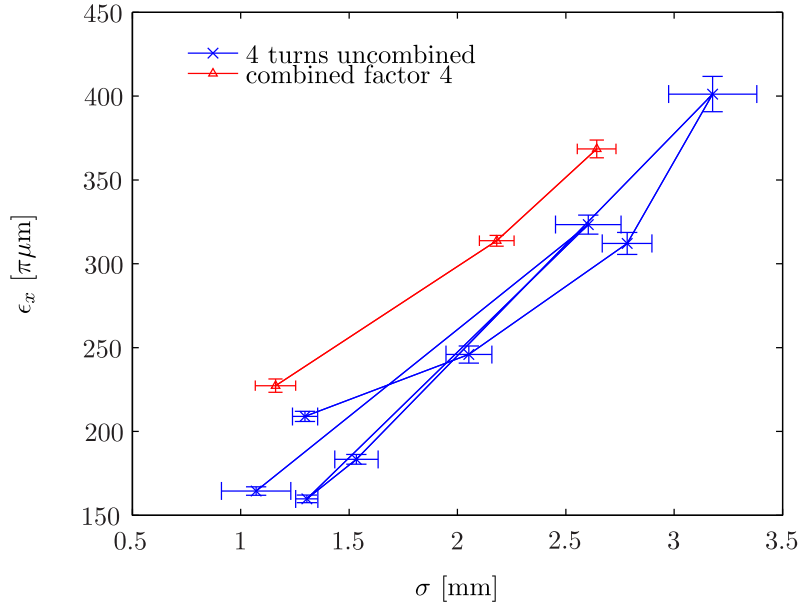


Figure 7.4: The horizontal emittance as a function of amplitude of the oscillations around the closed orbit.

a Drive Beam emittance of  $150 \pi \mu\text{m}$  was achieved for a factor 4 combined beam. The result is presented in Paper VIII together with a summary of recent achievements in CTF3.

## 7.2 Beam Stability at CTF3

The beam stability presented in this section will refer to a 3 GHz beam.

### 7.2.1 Motivation

The motivation to improve the beam stability in CTF3 is twofold. First, it is part of the feasibility demonstration for CLIC. The two-beam acceleration concept sets very tight constraints on the Drive Beam stability, described in section 6.1.2. The technical equipment is, however, significantly different in CTF3 compared to what is foreseen for CLIC. As a consequence it is not possible to achieve all the requirements in CTF3. The other motivation to improve the beam stability is to provide better experimental conditions for the other tests done at CTF3. This includes the two-beam acceleration and the deceleration tests. It also contributes to a better environment for further beam development such as optics studies.

### 7.2.2 Relation to CLIC

The nanometer level beam size at the collision points in CLIC puts tight constraints on the stability of RF production with the Drive Beam. The variation of the Drive Beam intensity, phase and bunch length will give rise to amplitude and phase errors of the accelerating RF. As a consequence energy errors will be introduced in the Main Beam. This can be translated into luminosity decrease in two different ways: first through the limited bandwidth of the beam delivery system and secondly through emittance increase caused by the energy error in the main linac [72]. The tolerances deriving from the two mechanisms are very similar. The maximum allowed beam current variation for CLIC is  $\frac{\sigma_I}{I} = 7.5 \times 10^{-4}$ .

### 7.2.3 Beam Current Variation

The beam current stability in the linac was demonstrated to be  $\frac{\sigma_I}{I} = 3 \times 10^{-4}$ , which is better than the CLIC specifications [77, 78]. After the beam exited the linac the beam current variation started to appear. An extensive study of these losses was launched and the main variation was found to derive from beam energy variation coming from the compressed RF-amplitude. The progress of this study and the methods implemented to mitigate these instabilities are presented in Paper VII. The full description of the study and the implemented feedback systems resulting in a beam current stability of below  $\frac{\sigma_I}{I} = 1 \times 10^{-3}$  for a beam combined 4 times are presented in Paper VI.

### 7.2.4 Phase and Bunch Length Variation

The phase of the beam is defined as the relative phase compared to a reference signal. The bunch length is the length of an individual bunch. This is illustrated in figure 7.5 which shows a part of a bunch train together with a reference signal. The phase of the beam in the linac is mainly determined by the phase of the RF fields in the injector. This means that the phase stability of the two first klystrons plays a very important role for the phase of the beam. In the beginning of the linac there are two phase monitors. They pick up the signal induced by the beam and compare it to a 3 GHz reference source. Using these two pickups a feedback was implemented to stabilize the beam phase further. The implemented feedback is described in Paper VIII. The performance of the feedback was also evaluated in phase monitors after the linac. The feedback decreased the phase variation of almost 40%. The feedback was also observed to improve the stability of the bunch length.

The phase stability after the stretching chicane (for location of chicane see figure 7.1) is also influenced by the energy variation and it strongly depends on the setting of the chicane. If no quadrupoles are powered, the chicane has a natural  $R_{56}$ . In CTF3 this corresponds to  $R_{56} = -0.45$ . This setting introduces an energy to path length dependency. This can be understood by looking at

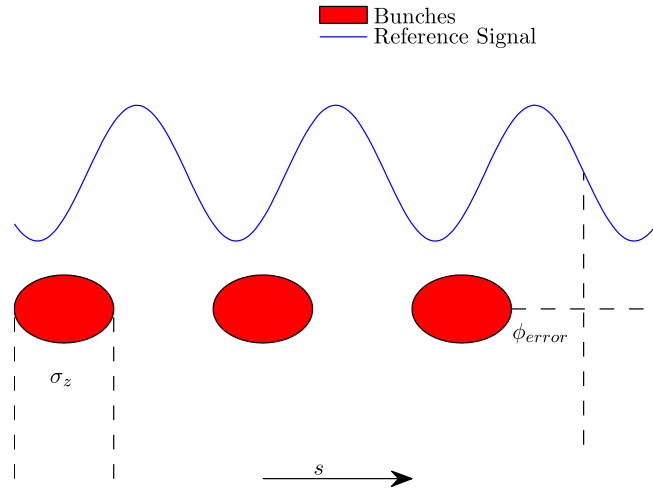


Figure 7.5: A part of a bunch train together with a reference signal. The phase error is defined as the phase variation compared to the reference signal. The bunch length ( $\sigma_z$ ) is the length of a individual bunch.

a magnetic chicane without any quadrupoles. Assume that the first pulse has 1% higher energy than the second. With a  $R_{56} = -0.45$  it will need to travel 0.45 mm shorter than the less energetic pulse. Travelling almost at the speed of light, this gives a time difference of  $1.5 \times 10^{-11}$  s. At 12 GHz this is a phase variation of  $65^\circ$ . In 2012 various optics were tested with lower  $R_{56}$  values [79]. The different optics were used to investigate the influence on the beam phase stability. The results are summarized in Paper VIII.

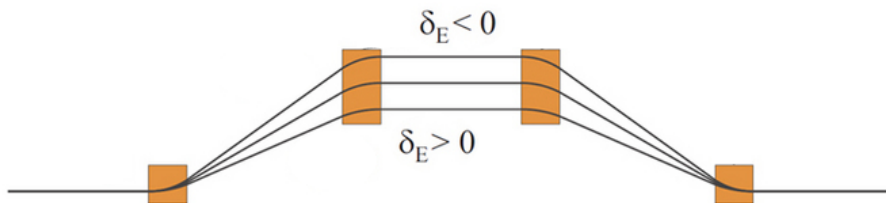


Figure 7.6: The different paths taken by particles with different energies.

### 7.3 Two-beam Acceleration

The two-beam acceleration takes place in TBTS. The beam is decelerated in a dedicated cavity called Power Extraction Structure (PETS). When the beam passes through the PETS structure it excites strong electromagnetic oscillations. In this way the beam converts its kinetic energy to electromagnetic

energy. This RF energy is extracted from the PETS and sent via waveguides to the accelerating structures. The PETS and the accelerating structures are travelling-wave structures, but with different parameters [80].

One of the strengths of CTF3 is its ability to create different beam current levels. This is done by shortening the pulse so that the beam instead combines 2 or 3 times, or is even sent straight, in the combiner ring. In this way we can also change the produced power in the PETS structure and hence change the power sent to the accelerating structure in TBTS. This method was used to probe different accelerating gradients in TBTS. A data acquisition system was also developed to combine the energy measurements of the CALIFES beam with the RF signals. The signals were not synchronized but through keeping stable conditions and averaging over several signals the relation between the produced RF-power and the acceleration was obtained. A description of the demonstration of the two-beam acceleration done at CTF3 can be found in Paper IX.

# Chapter 8

## Conclusion and Outlook

In this thesis beam-based methods to identify errors and drifts of important parameters in particle accelerators have been described. They have been developed to meet the challenging requirements of modern particle accelerators. The LHC is the first collider with strict requirements on the maximum deviation from the model in terms of  $\beta$ -functions. The acceptable peak  $\beta$ -beating for the horizontal plane is 19% and 15% for the vertical plane and it is desired to keep the  $|C^-|$  below 0.01. The correction procedures of the LHC optics, which resulted in an unprecedented low  $\beta$ -beat for a hadron collider of  $(7 \pm 4)\%$ , has been described. The robustness of the techniques has been demonstrated through the ability to correct various optics well within the requirements. Special focus has been given to the dedicated corrections of the high- $\beta$  optics which were a necessary condition for the dedicated physics runs for the TOTEM and ALFA experiments in 2012.

The transverse coupling has been observed to vary with time in several colliders including the LHC. An automatic approach based on measurement of injection oscillations to correct coupling has been demonstrated in this thesis. It uses all available BPMs to reconstruct the  $f_{1001}$  along the machine in a model independent way. A correction is then automatically calculated and applied. This method was used in normal operation of the LHC in 2012 and it was demonstrated to have a better performance and be less time consuming than the manual corrections used previously. Since the approach is based on the injection oscillations it is limited to corrections of the injection optics. In order to correct the coupling at different energies the layout of new coupling feedback has been designed. It will be based on a new BPM system, which was primarily developed for precise orbit measurements close to the IPs. As a consequence the locations of the BPMs are not optimized for coupling measurements and an approach to combine the information from several independent BPMs to measure the coupling globally has been developed to maximize the  $C^-$  precision. Simulation indicates that this layout will be able to provide a precise measurement of the global coupling and hence provide the possibility to perform coupling corrections online. This system will significantly improve

the control of the coupling in the LHC.

The quality of the coupling measurements has been enhanced by improvements in reconstruction algorithms and an improved understanding of how to clean the data. SVD is a well established method to reduce the noise in TbT-data. It is demonstrated within this thesis that reducing the number of singular values in data cleaning introduces systematic errors in the coupling measurements. In the LHC case the systematic errors are negligible if more than 8 singular values are used for the reconstruction. This number may vary depending on the BPM configuration and number of modes in the machine.

Two BPMs are needed to reconstruct  $f_{1001}$  and  $f_{1010}$  from TbT-data without any assumption on their relative amplitude. Two consecutive BPMs are commonly selected. In this thesis it is shown that selecting two BPMs with a phase advance close to  $\frac{\pi}{2}$  reduces the uncertainty of the reconstructed coupling by factor  $\sim 2$  compared to selecting consecutive BPMs. This is of particular importance close to the IPs since the phase advance between two consecutive BPMs normally is far from  $\frac{\pi}{2}$ . Performing the SVD cleaning and optimally selecting the BPM pair used to reconstruct the transverse momentum reduces the noise induced deviation by a factor  $\sim 3$ . Since the pairing improves the reconstruction of the transverse momentum it could also be used to improve the measurement quality of other RDTs.

A new method to measure and correct chromatic coupling based on the TbT has been presented. The energy is changed and the effect on the  $f_{1001}$  is measured. The chromatic coupling is then calculated and a correction using the skew sextupoles is applied. The reduction of the chromatic coupling was successfully applied to both LHC beams resulting in a reduction in chromatic coupling of a factor  $2.5 \pm 0.4$  for Beam 1 and  $1.6 \pm 0.3$  for Beam 2. The next step is to include these corrections in the regular operation of the LHC and to study its impact on, for example, the dynamic aperture.

The described measurements and corrections of the LHC optics have played a significant role in the excellent performance and results of the LHC. The goal when the machine is switched on in 2015 is to continue to narrow down the properties of the Higgs particle as well as looking for new physics. However, it is clear that it will be hard for the LHC to measure precisely enough all the crucial parameters of the Higgs boson [81]. Such detailed studies could instead be performed for example at CLIC. The beam parameters for CLIC are in general even more challenging than for the LHC and in many cases the requirements are beyond state-of-the-art. As a consequence it is necessary to demonstrate the ability to control the parameters to the required level in order for CLIC to be a feasible option as a next generation collider. In this thesis I have demonstrated methods developed and applied to CTF3 to achieve the required level of control in several relevant beam parameters. The identification process revealing the main causes for the drive beam drifts has been described. The main source of the energy variations was identified as drifts in the RF-power caused by a detuning of the RF compression cavities used in CTF3. A feedback operating on

---

the phase program of each klystron in order to stabilize the amplitude has been implemented. Working together with a dedicated energy feedback operating on the last klystron in the linac it reduces the energy variation with a factor 3. The feedbacks developed to automatically control of the pulse compression have demonstrated the ability to reach good beam stability with this system. The improved beam energy stability has significantly improved the beam current stability which today is very close to the CLIC requirement of  $\frac{\sigma_I}{I} = 7.5 \times 10^{-4}$  and hence played a role in the direct experimental demonstration of a crucial CLIC parameter.

The phase stability has also been improved by a dedicated beam-based feedback operating on klystrons in the CTF3 injector. The phase variation originating from the injector demonstrated a reduction of 40%.

The increased stability is crucial for all studies carried out at CTF3 as it permitted more accurate and reproducible measurements, which can be performed faster to reach the same precision. It yielded reproducible conditions crucial for quick machine setup, leaving more time for the experiments. Finally, it reduced the overall beam losses to levels that permitted increasing drive beam repetition rate by a factor 6. This was of great importance for break down rates measurements performed in TBTS.

The generation of the Drive Beam at design emittance, for a beam combined 4 times in the combiner ring, has been achieved. This was the result of beam optimization and studies of the influence on the emittance of oscillations around the closed orbit.

The unique concept of the two-beam acceleration, upon which the CLIC concept relies, has been successfully demonstrated in CTF3, at the nominal CLIC gradient of 100 MV/m and above. The acceleration as a function of the power has been investigated through beam-based studies.

A following step for CTF3 in its mission towards the demonstration of the CLIC technology is to achieve similar beam stability and emittance for a beam combined 8 times. In order to achieve this, an improved control of the orbit and the injector which is modified to produce the 1.5 GHz beam will be needed.

The overall goal of this thesis has been to develop and improve methods and algorithms which increase the performance and the understanding of particle accelerators. The different methods have been applied successfully to the LHC and CTF3 but also have potential applications in other present and future particle accelerators.



# Chapter 9

## Abbreviations and Acronyms

<b>ALFA</b>	Absolute Luminosity For Experiment
<b>ALICE</b>	A Large Ion Collider Experiment
<b>ATLAS</b>	A Toroidal LHC Apparatus
<b>BBQ</b>	diode-based base-band-tune
<b>BPM</b>	Beam Position Monitor
<b>CERN</b>	European Organization for Nuclear Research
<b>CLEX</b>	CLIC Experimental Area
<b>CLIC</b>	Compact Linear Collider
<b>CMS</b>	Compact Muon Solenoid
<b>CTF3</b>	CLIC Test Facility 3
<b>DOROS</b>	Diode Orbit and Oscillation
<b>FIDeL</b>	Field Description for the LHC
<b>GUI</b>	Graphical User Interface
<b>IP</b>	Interaction Point
<b>LEP</b>	Large Electron Positron
<b>LHC</b>	Large Hadron Collider
<b>LHCb</b>	LHC beauty
<b>OMC</b>	Optics Measurement and Correction
<b>PETS</b>	Power Extraction Structure
<b>PS</b>	Proton Synchrotron
<b>PTC</b>	Polymorphic Tracking Code
<b>RDT</b>	Resonance Driving Term
<b>RF</b>	Radio Frequency
<b>SPS</b>	Super Proton Synchrotron
<b>SVD</b>	Singular Value Decomposition
<b>TBL</b>	Test Beam Line
<b>TBTS</b>	Two Beam Test Stand
<b>TbT</b>	turn-by-turn
<b>TOTEM</b>	Total elastic and diffractive cross-section measurement



# Bibliography

- [1] The Royal Swedish Academy of Sciences. Press release of the nobel prize. [http://www.nobelprize.org/nobel\\_prizes/physics/laureates/2013/press.html](http://www.nobelprize.org/nobel_prizes/physics/laureates/2013/press.html).
- [2] *Large Hadron Collider in the LEP Tunnel*, Lausanne, Switzerland, 1984. <http://cds.cern.ch/record/154938/files/CERN-84-10-V-1.pdf>.
- [3] High energy physics advisory panel DOE/NSF. *Discovering the Quantum Universe, The role of Particle colliders*.
- [4] O. Brüning, P. Collier, P. Lebrun, S. Myers, R. Ostojic, J. Poole, and P. Proudlock. *LHC Design Report vol I, Chapter 3*. CERN, Geneva, 2004.
- [5] O. Brüning, P. Collier, P. Lebrun, S. Myers, R. Ostojic, J. Poole, and P. Proudlock. *LHC Design Report vol III*. CERN, Geneva, 2004.
- [6] CERN. Large Hadron Collider reaches record 1380 proton bunches per beam, 2012. <http://phys.org/news/2012-04-large-hadron-collider-proton-bunches.html>.
- [7] *ATLAS detector and physics performance: Technical Design Report, 2*. Technical Design Report ATLAS. CERN, Geneva, 1999.
- [8] CMS Collaboration. CMS physics: Technical design report volume 2: Physics performance. *J. Phys. G*, 34(CERN-LHCC-2006-021. CMS-TDR-8-2):995–1579. 669 p, 2007. Submitted on 2006-09-22.
- [9] *LHCb : Technical Proposal*. Tech. Proposal. CERN, Geneva, 1998.
- [10] P. Cortese, W. Fabjan, L. Riccati, K. Safarik, and H. de Groot. *ALICE physics performance: Technical Design Report*. Technical Design Report ALICE. CERN, Geneva, 2005. revised version submitted on 2006-05-29.
- [11] S. Brewster. First proton-lead collision test at the LHC successful. *Symmetry*, September 2012.
- [12] V. Berardi et al. *Total cross-section, elastic scattering and diffraction dissociation at the Large Hadron Collider at CERN: Addendum to the*

- 
- TOTEM Technical Design Report*. Technical Design Report TOTEM. CERN, Geneva, 2004. Submitted on 18 Jun 2004.
- [13] P. Jenni, M. Nordberg, M. Nessi, and K. Jon-And. *ATLAS Forward Detectors for Measurement of Elastic Scattering and Luminosity*. Technical Design Report. CERN, Geneva, 2008.
- [14] T. Feder. World lays groundwork for future linear collider. *Physics Today*, 63(7):22–24, 2010.
- [15] Nobelprize.org. Nobel Media AB 2013. The nobel prize in physics 1984, 1999. [http://www.nobelprize.org/nobel\\_prizes/physics/laureates/1984/](http://www.nobelprize.org/nobel_prizes/physics/laureates/1984/).
- [16] ALEPH Collaboration. Determination of the number of light neutrino species. *Physics Letters B*, 231(4):519 – 529, 1989.
- [17] H. Wiedemann. *Particle Accelerator Physics*. Springer, third edition.
- [18] F. Tecker. Future linear colliders. Summer student lecture, 2010.
- [19] A multi-teV linear collider based on CLIC technology, CLIC conceptual design report. Technical Report CERN-2012-007, CERN, Geneva, May 2012.
- [20] ILC technical design report. Technical report, 2013. <http://www.linearcollider.org/ILC/Publications/Technical-Design-Report>.
- [21] F. Zimmermann, A. P. Blondel, M. Koratzinos, and M. Zanetti. TLEP: A high-performance circular  $e^+ e^-$  collider to study the higgs boson. In *IPAC'13, Shanghai, China*, 2013.
- [22] CMS Collaboration. Search for top squarks in r-parity-violating supersymmetry using three or more leptons and b-tagged jets. *Submitted to PRL*, (arXiv:1306.6643 [hep-ex]), 2013. <http://arxiv.org/abs/1306.6643>.
- [23] S. Y. Lee. *Accelerator physics*. World Scientific, 2004.
- [24] R. Tomás. *Direct Measurement of Resonance Driving Terms in the Super Proton Synchrotron (SPS) of CERN using Beam Position Monitors*. PhD thesis, Valencia U., València, 2003. Presented on 30 Mar 2003.
- [25] M. G. Minty and F. Zimmermann. *Measurement and Control of Charged beams*. Springer, 2003.
- [26] R. Capii and M. Giovannozzi. Multiturn extraction and injection by means of adiabatic capture in stable islands of phase space. *Phys. Rev. Spec. Top. Accel. Beams*, 7(024001), 2004.

- [27] M. Giovannozzi and J. Morel. Principle and analysis of multiturn injection using stable islands of transverse phase space. *Phys. Rev. Spec. Top. Accel. Beams*, 10(034001), 2007.
- [28] R. Tomás. From Farey sequences to resonance diagrams. *Phys. Rev. ST Accel. Beams*, 17:014001, Jan 2014.
- [29] X. Shen. 2d resonance diagram from farey sequence. [http://mypage.iu.edu/~xiaoshen/Files/NumericalTools/Resonance\\_diagram\\_Farey\\_sequence/2d\\_Resonance\\_Diagram\\_from\\_Farey\\_Sequence.tar.gz](http://mypage.iu.edu/~xiaoshen/Files/NumericalTools/Resonance_diagram_Farey_sequence/2d_Resonance_Diagram_from_Farey_Sequence.tar.gz).
- [30] J. Liouvilles. *Journ. de Math.*, pages 3, 349, 1838.
- [31] E. D. Courant and H. S. Snyder. Theory of the alternating gradient synchrotron. *Annals of Physics*, pages 3:1–48, 1958.
- [32] R. E. Meller, A. W. Chao, J. M. Peterson, S. G. Peggs, and M. Furman. Decoherence of kicked beams. Technical Report SSC-N-360, 1987.
- [33] L. C Teng. Concerning n-dimensional coupled motions. Technical report, 1971. FN-229.
- [34] F. Willeke and G. Ripken. Methods of beam optics. Technical report, 1988. DESY 88-114.
- [35] O. Brüning and S. Fartoukh. Field quality specification for the lhc main dipole magnets. Technical Report LHC-Project-Report-501. CERN-LHC-Project-Report-501, CERN, Geneva, Oct 2001.
- [36] J. Serrano and M. Cattin. The LHC ac dipole system: an introduction. May 2010.
- [37] R. Miyamoto. Diagnostics of the Fermilab Tevatron using an AC dipole. 2008.
- [38] R. Tomás. Normal form of particle motion under the influence of an ac dipole. *Phys. Rev. ST Accel. Beams*, 5:054001, May 2002.
- [39] R. Bartolini and F. Schmidt. A computer code for frequency analysis of non-linear betatron motion. Technical report, 2013. SL-Note-98-017-AP.
- [40] R. Tomas et al. Procedures and accuracy estimates for beta-beat correction in the LHC. In *EPAC'06, Edinburgh, Scotland*, 2006.
- [41] R. Calaga et al. Beta star measurement in the LHC based on k-modulation. In *IPAC'11, San Sebastian, Spain*, 2011.

- 
- [42] A. Boccardi, M. Gasior, R. Jones, P. Karlsson, and R. Steinhagen. First results from the LHC BBQ tune and chromaticity systems. Technical Report LHC-Performance-Note-007. CERN-LHC-Performance-Note-007, CERN, Geneva, Jan 2009.
- [43] R. Calaga, R. Tomas, and F. Zimmermann. BPM calibration independent LHC optics correction. In *PAC07, Albuquerque, New Mexico, USA*, number CERN-ATS-2012-136, 2007.
- [44] M. Aiba, S. Fartoukh, A. Franchi, M. Giovannozzi, V. Kain, M. Lamont, R. Tomás, G. Vanbavinckhove, J. Wenninger, F. Zimmermann, R. Calaga, and A. Morita. First beta-beating measurement and optics analysis for the CERN Large Hadron Collider. *Phys. Rev. ST Accel. Beams*, 12:081002, Aug 2009.
- [45] MAD-X. <http://mad.web.cern.ch/mad/>.
- [46] V. Glenn. *Optics measurements and corrections for colliders and other storage rings*. PhD thesis, Amsterdam U., Jan 2013. Presented 16 Jan 2013.
- [47] H. Burkhardt, S. Cavalier, G. Muller, S. Redaelli, R. Tomás, G. Vanbavinckhove, J. Wenninger, and S. White. 90m optics studies and operation in the LHC. In *IPAC'12, New Orleans, USA*, 2012.
- [48] G. Ripken and F. Willeke. On the impact of linear coupling on nonlinear dynamics. *Part. Accel.*, 27(DESY-90-001):203–208. 41 p, Jan 1990. <http://cds.cern.ch/record/204506/files/p203.pdf>.
- [49] G. Guignard. Betatron coupling and related impact of radiation. *PYHYSICAL REVIEW E*, 51(6), 1995.
- [50] A. Franchi. *Studies and Measurements of Linear Coupling and Nonlinearities in Hadron Circular Accelerators*. PhD thesis, Universität Frankfurt, 2006. [http://www.gsi.de/en/start/beschleuniger/fachabteilungen/accelerator\\_physics/phd\\_thesis.htm](http://www.gsi.de/en/start/beschleuniger/fachabteilungen/accelerator_physics/phd_thesis.htm).
- [51] F. Zimmermann and M. Minty. Measurement of betatron coupling at the atf damping ring. Technical report. <http://atfweb.kek.jp/atf/Reports/ATF-98-22>.
- [52] P. J. Bryant. A simple theory for weak betatron coupling. 1994. <http://cds.cern.ch/record/261066/?ln=en>.
- [53] A. Franchi. Coupling correction through beam position data. <https://indico.cern.ch/getFile.py/access?contribId=11&sessionId=10&resId=0&materialId=slides&confId=148596>.

- [54] D. D. Caussyn, M. Ball, B. Brabson, J. Collins, S. A. Curtis, V. Derenchuck, D. DuPlantis, G. East, M. Ellison, T. Ellison, D. Friesel, B. Hamilton, W. P. Jones, W. Lambie, S. Y. Lee, D. Li, M. G. Minty, T. Sloan, G. Xu, A. W. Chao, K. Y. Ng, and S. Tepikian. Experimental studies of nonlinear beam dynamics. *Phys. Rev. A*, 46:7942–7952, Dec 1992.
- [55] A. Franchi, R. Tomás Garcia, and G. Vanbavinkhove. Computation of the Coupling Resonance Driving term f1001 and the coupling coefficient C from turn-by-turn single-BPM data. May 2010. <http://cds.cern.ch/record/1264111?ln=en>.
- [56] R. Bartolini and F. Schmidt. Sussix: a computer code for frequency analysis of non-linear betatron motion. Technical report, 2010. CERN SL/Note 98-017 (AP) <https://cds.cern.ch/record/702438/files/>.
- [57] R. Tomás, M. Bai, R. Calaga, W. Fischer, A. Franchi, and G. Rumolo. Measurement of global and local resonance terms. *Phys. Rev. ST Accel. Beams*, 8:024001, Feb 2005.
- [58] A. Franchi, R. Tomás, and F. Schmidt. Magnet strength measurement in circular accelerators from beam position monitor data. *Phys. Rev. ST Accel. Beams*, 10:074001, Jul 2007.
- [59] R. Tomás, O. Brüning, M. Giovannozzi, P. Hagen, M. Lamont, F. Schmidt, G. Vanbavinckhove, M. Aiba, R. Calaga, and R. Miyamoto. CERN Large Hadron Collider optics model, measurements, and corrections. *Phys. Rev. ST Accel. Beams*, 13:121004, Dec 2010.
- [60] R. Tomás. Optimizing the global coupling knobs for the lhc, Feb 2012. <http://cds.cern.ch/record/1422434>.
- [61] A. Boccardi, M. Gasior, R. Jones, P. Karlsson, and R. Steinhagen. First Results from the LHC BBQ Tune and Chromaticity Systems. Technical Report LHC-Performance-Note-007. CERN-LHC-Performance-Note-007, CERN, Geneva, Jan 2009. <http://cds.cern.ch/record/1156349/files/performance-note-007.pdf>.
- [62] T. Persson. Automatic coupling correction, 2013. <http://indico.cern.ch/event/246159/session/1/contribution/13/material/slides/1.pdf>.
- [63] T. Persson. Coupling feedback, 2012. <http://rtomas.web.cern.ch/rtomas/LHCOptics/>.
- [64] J.-P. Koutchouk. Chromatic Properties of the LHC Lattice Version 5.0 at Injection. Technical Report CERN-LHC-Project-Note-113, CERN, Geneva, Oct 1997. <http://cdsweb.cern.ch/record/691854>.

- 
- [65] S. D. Fartoukh. Chromatic Coupling Induced by Skew Sextupolar Field Errors in the LHC Main Dipoles and its Correction. Technical Report CERN-LHC-Project-Report-278, CERN, Geneva, Mar 1999.
- [66] S. D. Fartoukh and J.-P. Koutchouk. Chromatic coupling in LHC and its correction. In *EPAC'00 Vienna, Austria*, number CERN-LHC-Project-Report-400, page 4 p, Aug 2000.
- [67] S. D. Fartoukh and M. Giovannozzi. Dynamic aperture computation for the as-built CERN Large Hadron Collider and impact of main dipoles sorting. *Nuclear Instruments and Methods in Physics Research Section A: Accelerators, Spectrometers, Detectors and Associated Equipment*, 671(0):10–23, 2012.
- [68] Y. Ohnishi, K. Ohmi, H. Koiso, M. Masuzawa, A. Morita, K. Mori, K. Oide, Y. Seimiya, and D. Zhou. Measurement of chromatic  $x$ - $y$  coupling. *Phys. Rev. ST Accel. Beams*, 12:091002, Sep 2009.
- [69] D. Zhou, K. Ohmi, Y. Seimiya, Y. Ohnishi, and A. Morita. Simulations on beam-beam effect under the presence of general chromaticity. Technical Report 2009-10, May 2009.
- [70] E. Adli. *A Study of the Beam Physics in the CLIC Drive Beam Decelerator*. PhD thesis, Oslo, Norway, U. Oslo, 2009. Presented on 03 Nov 2009.
- [71] A. Grudiev, H. H. Braun, D. Schulte, and W. Wuensch. Optimum frequency and gradient for the CLIC MAIN linac accelerating structure. In *LINAC'08, Victoria, BC, Canada*, 2008.
- [72] D. Schulte and R. Tomas. Dynamic effect in the new CLIC main linac. In *PAC'09 Vancouver, BC, Canada*, 2009.
- [73] R. Corsini et al. First full beam loading operation with the CTF3 linac. In *EPAC'04, Lucerne, Switzerland*, 2004.
- [74] G. Geschonke and A. Ghigo. CTF3 design report. oai:cds.cern.ch:559331. Technical Report CERN-PS-2002-008-RF. CTF-3-NOTE-2002-047. LNF-2002-008-IR, CERN, Geneva, May 2002.
- [75] R. Corsini. Status and future of the CLIC study. In *LINAC'12, Tel-Aviv, Israel*, 2012.
- [76] P. Skowronski for the CTF3 Collaboration. CTF3 Drive Beam studies results and program. CLIC workshop 2013, Geneva, Switzerland.<http://indico.cern.ch/getFile.py/access?contribId=162&sessionId=29&resId=1&materialId=slides&confId=204269>, 2013.
- [77] D. Schulte et al. Status of the CLIC phase and amplitude stabilization concept. In *LINAC'10, Tsukuba, Japan*, 2010.

- [78] T. Persson. Fighting beam instabilities at CTF3. Master's thesis, Chalmers University of Technology, 2011.
- [79] J. Barranco. Low momentum compaction and bunch lengths. CLIC workshop 2013, Geneva, Switzerland. <http://indico.cern.ch/getFile.py/access?contribId=164&sessionId=29&resId=0&materialId=slides&confId=204269>, 2013.
- [80] H. Braun, J. Delahaye, A. Roeck, and G. Geschonke. CLIC here for the future. *CERN Courier*, August 2008. <http://cerncourier.com/cws/article/cern/35450>.
- [81] M. Peskin, 2013. LCWS Workshop 2013, Tokyo, Jpn. <http://agenda.linearcollider.org/getFile.py/access?contribId=9&sessionId=11&resId=0&materialId=slides&confId=6000>.
- [82] E. Forest, M. Berz, and J. Irwin. Normal form methods for complicated periodic systems: a complete solution using differential algebra and lie operators. *Part. Accel.*, 24:91–107, 1989.



# Acknowledgment

The journey to a complete PhD is long and it is difficult to know where to begin the story. When I start to think about how it all came to happen I see that there are a lot of people who have played smaller and bigger roles all the way from elementary school to present day. I will not be able to mention all of you but you are not forgotten!

I would like to start with giving my sincere thanks to Piotr Skowronski who introduced me to the world of accelerators and has helped me ever since. Your knowledge and ability to always answer my questions has been a prerequisite for this thesis. It has been a joy to have you as my supervisor. I would also like to thank you for bringing me with you when you were invited to work for the LHC.

My sincere gratitude also goes to Rogelio Tomás for accepting to supervise my work related to the LHC. You always find time to answer my question even when I can see that you are extremely busy. This also includes getting answers to emails in the middle of the night and during weekends. It has been a pleasure to work with and learn from such a dedicated expert.

I also would like to thank Thomas Nilsson for being my university supervisor since the bachelor thesis. Without the interest I got for science when I was writing the bachelor thesis I would not have pursued a PhD. Also many thanks for guidance and for sorting out all the requirements from the university side.

I would also like to thank the entire OMC team and in particular Yngve Levinsen, Glenn Vanbavinckhove and Ewen Maclean. You really made me feel welcome in the team and took the time to explain how everything worked. Thank you Ewen for the discussions we have had involving beam physics and life in general. Many thanks for helping out with proofreading. To Yngve: It has been a delight for me to collaborate closely with you, both in the OMC team and with the chromatic coupling. Also I have really enjoyed the coffee breaks and the discussions we have. I wish you all the best in the future!

Thanks also to Andrea Franchi who has, even though we just met very briefly, provided very useful input through emails on problems related to coupling.

I would like to thank all the members of the CTF3 team for their patience while the feedbacks were still in a testing phase. Thank you Ben Constance for discussions about the feedbacks and for proofreading parts of this thesis. Also

a big thanks to Roberto Corsini and Frank Tecker for valuable ideas on how to find and mitigate instabilities in CTF3.

On a personal level I would like to thank my friends in the Geneva region Foteini Asvesta, Javier Barranco, Davide Gamba, Alexander Gerbershagen, Ole Hansen, Lars Hedlund, Reidar Lillestøl, Pieter Everaerts, Line Everaerts, Juha Kemppinen, Andriy Nosych, Daria Nosych, Marcus Palm, Theo Rutter, Jochem Snuverink, Christina Yin Vallgren and many others for great moments both at CERN and outside in the real world.

I would also like to thank everyone in the Weirdo team: Jonathan Karlsson, Viktor Kämpe, Hampus Linander, Oscar Landgren, Lukas Lindroos, Magnus Sandén, Kajsa Sols, Anton Sörensen, Ronja Theis, Eskil Varenius. I loved the lunches we had during our years at the university, the times we studied and the times when we played computer games when we should have been studying. I am so glad that we still manage to meet from time to time.

I am also very grateful to have friends in Sweden: Alborz Tavosian, Viktor Nord, Fredrik Göthensten, Michael Svensson, Joakim Rosén and Elliot Bavarian. You have provided a base for me to come back to when I am in Sweden where things other than science and accelerators matter.

Other people in Sweden that I am grateful to have are: Kjell Hermansson and Peter Persson.

To all my friends, I am so glad to have you!

My gratitude also goes to Annelie for moving far away from her siblings and parents down here. I know it has been a true sacrifice and I will always be grateful. Also many thanks for proofreading most of the things I have ever written in an academic context.

Finally, I would like to thank my parents for their never ending support no matter which choices I make in life. Also a big thanks for always being happy to see me without giving me feelings of guilt when I leave. Thank you for always being there for me!

# Appendix A

## Resonance Driving Terms

The derivation in this section follows the approach given in [24, 50]. The non-linear dynamics can not be described by matrices but may be described by the transfer maps formalism. It has been shown that in a the frame where the one turn map is represented by a pure rotation, it may be written as [24]

$$\mathcal{M} = e^{:\tilde{h}_1:} e^{:\tilde{h}_2:} \dots e^{:\tilde{h}_n:} R \quad , \quad (\text{A.1})$$

where  $e^{:\tilde{h}_n:}$  is an exponential Lie operator describing a non linear element and  $R$  is the rotation matrix describing the linear motion. Using Campbell-Baker-Hausdorff theorem this simplifies to  $\mathcal{M} = e^{:h:} R$ . In case  $\tilde{h}_n$  are small  $h$  may be approximated as

$$h = \sum_{n=1}^N \tilde{h}_n + \sum_{n,m < n}^N [\tilde{h}_m, \tilde{h}_n] + \dots \quad (\text{A.2})$$

Using only the first order in  $\tilde{h}_n$ ,  $h$  may be expanded according to Eq. (A.3) [24, 50] using the action angle variables described in Eq. (A.8).

$$h = \sum_{jklm} h_{jklm} (2J_x)^{\frac{j+k}{2}} (2J_y)^{\frac{l+m}{2}} e^{i[(j-k)(\phi_x - \phi_{x_0}) + (l-m)(\phi_y - \phi_{y_0})]} \quad (\text{A.3})$$

$h_{jklm}$  are Hamiltonian coefficients containing contributions from all multipoles of order  $n = j + k + l + m$ . A multipole of order  $n$  gives rise to terms in the Hamiltonian  $\propto x^{j+k} y^{l+m}$ , where  $n = j + k + l + m$ .

In case of a skew quadrupole it gives rise to the terms in the Hamiltonian  $\propto xy$ , meaning that it contributes to  $h_{1010}$ ,  $h_{1001}$ ,  $h_{0110}$  and  $h_{0101}$ . The next step is to change to coordinates that shapes the map into a simpler form. The idea behind normal form coordinates is to perform a transformation from a system with amplitude and phase dependence to a simpler form. The simplest form is an amplitude dependent rotation, i.e. a rotation in phase space where the angle depends on the amplitude of the particle.

The coordinate change is represented by a similarity transformation of the one turn map

$$e^{-:F:} e^{:h:} R e^{:F:} \quad , \quad (\text{A.4})$$

where  $F$  is the generating function for the transformation. The formal solution to finding the generating function  $F$  is given in [82] and the explicit expression is obtained in [24] as

$$F = \sum_{jklm} f_{jklm} (2I_x)^{\frac{j+k}{2}} (2I_y)^{\frac{l+m}{2}} e^{i[(j-k)(\psi_x - \psi_{x_0}) + (l-m)(\psi_y - \psi_{y_0})]} \quad , \quad (\text{A.5})$$

where  $f_{jklm}$  are the resonance driving terms which correspond to  $h_{jklm}$  according to Eq.(A.6) [24, 50], where  $Q_x$  and  $Q_y$  are the unperturbed tunes.

$$f_{jklm} = \frac{h_{jklm}}{1 - e^{i2\pi[(j-k)Q_x + (l-m)Q_y]}} \quad (\text{A.6})$$

Eq. (A.6) diverges when  $j, k, l, m, Q_x$  and  $Q_y$  satisfy Eq. (2.24). Hence  $f_{jklm}$  are the driving terms of resonances  $[(j-k), (l-m)]$ .

$$(j-k)Q_x + (l-m)Q_y = p \quad \text{where } p \in \mathcal{Z} \quad (\text{A.7})$$

Every Hamiltonian term is associated with a resonance which explains the name Resonance Driving Terms.

The normalized Courant-Snyder coordinates are related to the action-angle variable as

$$\begin{aligned} z &= \sqrt{2J_z} \cos(\phi_z - \phi_{z_0}) \\ p_z &= -\sqrt{2J_z} \sin(\phi_z - \phi_{z_0}) \quad \text{where } z = x, y \end{aligned} \quad (\text{A.8})$$

It is convenient to introduce the resonant basis  $h$  defined as

$$\begin{aligned} h_z^\pm &= z \pm ip_z = \sqrt{2J_z} e^{\mp i(\phi_z - \phi_{z_0})} \quad \text{where } z = x, y \\ \mathbf{h} &= (h_x^+, h_x^-, h_y^+, h_y^-) \quad . \end{aligned} \quad (\text{A.9})$$

The transformation to a new set of Normal Form coordinates  $(\zeta_x^+, \zeta_x^-, \zeta_y^+, \zeta_y^-)$  is given by the operator  $e^{:-F:}$ . This is expressed as

$$\zeta_z^\pm = \sqrt{2I_z} e^{\pm i(\phi_z + \phi_{z_0})} = e^{:-F:} h_z^\pm \quad , \quad (\text{A.10})$$

where  $I_z$  is the invariant of motion in the new frame. The one-turn map in normal form coordinates is by construction an amplitude dependent rotation and hence the motion in these coordinates as a function of the turn number  $N$  is given by

$$\zeta_z^-(N) = \sqrt{2I_z} e^{2\pi\nu_x N + \phi_{z_0}} \quad . \quad (\text{A.11})$$

The inverse transformation from the new action-angle variables to the linearly normalized variable is to first order written as

$$h_z^- = e^{iF} \zeta_z^- \simeq \zeta_z^- + [F, \zeta_z^-] \quad (\text{A.12})$$

and using the Eq. (A.11) and Eq. (A.12) the normalized coordinates can be expressed in the form

$$\begin{aligned} h_x^-(N) &= \sqrt{2I_x} e^{i(2\pi\nu_x N - \psi_{x_0})} - \\ &\quad 2i \sum_{jklm} j f_{jklm} (2I_x)^{\frac{j+k-1}{2}} (2I_y)^{\frac{l+m}{2}} e^{i[(1-j+k)(2\pi\nu_x N - \psi_{x_0}) + (m-l)(2\pi\nu_y N - \psi_{y_0})]} \\ \\ h_y^-(N) &= \sqrt{2I_y} e^{i(2\pi\nu_y N - \psi_{y_0})} - \\ &\quad 2i \sum_{jklm} l f_{jklm} (2I_x)^{\frac{j+k}{2}} (2I_y)^{\frac{l+m-1}{2}} e^{i[(k-j)(2\pi\nu_x N - \psi_{x_0}) + (1-l+m)(2\pi\nu_y N - \psi_{y_0})]} \quad . \end{aligned} \quad (\text{A.13})$$

